Mon. Not. R. astr. Soc. (1989) **240,** 591–635

Low-luminosity radio sources in early-type galaxies

Elaine M. Sadler *European Southern Observatory, Karl-Schwarzschild-Str. 2, D-8046 Garching bei München, FRG and Kitt Peak National Observatory, PO Box 26732, Tucson, AZ 85726, USA*

C. R. Jenkins *Royal Greenwich Observatory, Hertsmonceux Castle, Hailsham, East Sussex BN27 1RP*

C. G. Kotanyi *National Radio Astronomy Observatory, PO Box 0, Socorro, New Mexico 87801, USA and Observatoire de Paris-Meudon, 92190 Meudon, France†*

Accepted 1989 March 14. Received 1989 March 14; in original form 1988 November 2

Summary. We have made a sensitive radio continuum survey of 114 nearby E and S0 galaxies to search for weak sources. The radio detection rate is 42 per cent, with a flux limit of 0.8 mJy at 5 GHz. By deriving the radio luminosity function for a complete sample, we show that most bright early-type galaxies have low-luminosity (10^{19}–10^{21} W Hz^{-1}) non-thermal radio sources.

Galaxies of similar optical luminosity vary widely in radio luminosity, but a characteristic radio power (the 30th percentile) rises roughly as the optical luminosity squared. S0 galaxies have weaker radio sources on average than elliptical galaxies, but this can be explained by the low luminosity of most S0 bulges relative to ellipticals. We find no correlation between radio power and axial ratio for galaxies with radio luminosities below 10^{23} W Hz^{-1}.

Most early-type galaxies have modest amounts of ionized gas in their central regions, but there is no correlation between optical emission-line luminosity and the presence or strength of radio emission at the low luminosities considered here.

1 Introduction

Early radio observations detected a number of large and powerful double-lobed radio sources associated with elliptical galaxies. Radio galaxies of this kind are rare objects, and we still understand very little about how they form and evolve.

Subsequent radio surveys with more sensitive flux limits have revealed weaker and less extended radio sources in many more galaxies, suggesting that a low level of radio emission is

★Present address: Anglo-Australian Observatory, PO Box 296, Epping, NSW 2121, Australia.
†Present address: Instituto de Pesquisas Espacias Radio INPE, CP 515, 12 201 São José dos Campos, Brazil.

common. Several studies of elliptical and S0 galaxies have found correlations between their radio and optical properties. The probability of radio emission in an early-type galaxy increases with optical luminosity, at least for the brightest galaxies (Auriemma *et al.* 1977). Elliptical galaxies appear to contain radio sources more often than S0s (Heeschen 1970; Dressel 1981; Hummel & Kotanyi 1982), galaxies with compact central sources often show [O II] λ3727 emission lines (Ekers & Ekers 1973; O'Connell & Dressel 1978) and radio emission may occur more often in round galaxies than in flat ones (Hummel, Kotanyi & Ekers 1983; Disney, Sparks & Wall 1984; but see also Dressel 1981).

These results are often interpreted in terms of the ability of galaxies to retain a supply of gas which can fuel an active nucleus (e.g. Gunn 1979). If such a mechanism is important, we might expect the radio properties of an elliptical galaxy to be related to its central gas content. Even small amounts of gas, if ionized, produce observable optical emission lines, but although there have been several radio surveys of E and S0 galaxies, there were until recently few homogeneous data on their emission-line properties.

In this paper, we use new radio observations of a complete sample of early-type galaxies (Sadler 1984a, b, c) and the results of a sensitive survey for optical emission lines of Hα and [N II] (Phillips *et al.* 1986) to discuss both the general properties of weak radio sources in early-type galaxies, and the relation between the gas content of the inner 1–2 kpc and the presence of a central radio source.

Section 2 of this paper describes the VLA observations, and we present a new derivation of the local radio luminosity function in Section 3. Sections 4 and 5 discuss the radio emission from nearby E and S0 galaxies. In Section 6 we examine the relation between central radio sources and optical emission lines, and Section 7 offers some conclusions and suggestions for further work.

A Hubble constant of 100 h km s^{-1} Mpc^{-1} is used throughout this paper, and we list here the corrections when h has a value other than 1:

Absolute magnitude:	$M_B(h) = M_B + 5\log(h)$,
Radio power:	$\log P(h) = \log P - 2\log(h)$,
Space density:	$\log \Phi(h) = \log \Phi - 3\log(h)$.

The distances used for galaxies in this study (listed in Table 4) were calculated using the radial velocity v_0 listed by Sadler (1984a) with the assumption that all galaxies are at their redshift distance, i.e. there are no peculiar velocities. We made no correction for infall to the Virgo cluster.

Recent work on the streaming motions of nearby galaxies (summarized, for example, by Lynden-Bell 1987) suggests that the structure of the local Hubble flow may in fact be very complex, with peculiar motions of several hundred km s^{-1} for galaxies in the region of the Centaurus cluster. We have nevertheless continued to use redshift distances for galaxies in this study, simply because we do not have enough information to make more elaborate corrections. Errors of up to 20–30 per cent in the distances of individual galaxies are unlikely to affect the major conclusions of this work.

2 VLA observations

2.1 THE VLA SAMPLE

A complete sample of 248 E and S0 galaxies south of declination $-32°$ and brighter than magnitude 14 (hereafter referred to as the Parkes sample) was surveyed at 2.7 and 5 GHz with the Parkes single-dish radio telescope by Sadler (1984c). The advantage of this sample over

those used in most previous radio studies was that it had well-defined selection criteria and a high level of optical completeness (90 per cent complete at $B_T = 13.8$). The detection rate at Parkes was 15 per cent, with a limit of 25 mJy at 2.7 GHz. To increase the detection rate and map the radio structure in the detected galaxies, further observations were made with the Very Large Array (VLA) synthesis radio telescope of the National Radio Astronomy Observatory (Thompson *et al.* 1980). The declination limit of the VLA restricted these observations to galaxies north of $-45°$ (hereafter, the VLA sample).

One hundred and nine galaxies were observed at 4.885 GHz (6 cm) duing a single 24-hr run in 1984 March. The VLA was in a hybrid B/C configuration which partly compensated for the beam distortion at southern declinations. The shortest interferometer spacing in this configuration was 63 m, so emission on scales larger than about 4 arcmin could not be detected. Each galaxy was observed for 5–10 min in a 'snapshot' mode with a typical 5σ detection limit of 0.8 mJy. The spatial resolution was 3–5 arcsec. Six galaxies originally scheduled (NGC 4645B, ESO 381-G12, NGC 4645, NGC 4696B, ESO 322-G102 and NGC 4706) were not observed because of a power failure during the observing run. Since they lay in the crowded Centaurus region, it was not possible to reschedule them during the short time remaining. Five galaxies in the sample (ESO 263-G48, NGC 4696, 5140, 7070A and 7097) had already been observed by Laing *et al.* (in preparation), who kindly provided their data in advance of publication. The two strong southern sources Centaurus A (NGC 5128) and Fornax A (NGC 1316) were not observed, since good maps are already available. The total VLA sample listed in Table 1 comprises 116 galaxies north of the $-45°$ declination limit. Morphological types and optical positions are from the ESO/Uppsala catalogue (Lauberts 1982). The last two columns give the total flux density measured from the VLA maps, and an indication of whether the source was spatially resolved, as well as its likely size.

2.2 DATA REDUCTION

Data reduction was done in the standard way. The maps were CLEANed, and an integrated flux density measured for each source. In a first pass, maps were made at a resolution of about 15 arcsec, using only the short interferometer spacings, in order to see extended emission more easily. Forty-nine galaxies were detected, and in 14 of these the radio emission extended over 15 arcsec or more.

Integrated flux densities from the VLA maps were found to be systematically lower than the Parkes single-dish measurements for galaxies detected in both surveys, and this may result from over-resolution of extended emission at the VLA. A comparison of the Parkes and VLA fluxes gave

$$\log S_{\mathrm{PKS}} \simeq \log S_{\mathrm{VLA}} + 0.1,$$

so, unless the VLA map showed a confusing source, the single-dish measurement was adopted as the total flux for galaxies with extended emission. For galaxies detected at the VLA but not at Parkes, no correction was made to the integrated VLA flux.

In a second pass, maps of the detected galaxies were made at full resolution. Except for NGC 3250 (which was detected at Parkes, but not at the VLA), all the galaxies with extended radio emission also had a central source (on a scale of a few arcsec or less) coincident with their nucleus. Five galaxies detected at Parkes (NGC 3268, ESO 323-G93, NGC 5140, NGC 6958 and IC 1459) remained unresolved at the VLA and four of these have flat or inverted radio spectra, in agreement with the well-known result that the radio emission from such galaxies is often dominated by a compact core (Heeschen 1970).

Table 1 lists the galaxies detected at the VLA, the measured total flux in each map and the approximate extent of radio emission. Table 2 lists core fluxes for the unresolved central sources of galaxies with extended radio emission. Where measurements with better spatial resolution were available from the literature, these have been substituted in column 3. Table 3 lists the radio and optical position angles, while Table 4 gives optical and radio data for the entire PKS/VLA galaxy sample. Two galaxies at very low galactic latitude, ESO 137-G08 and 137-G10 were excluded from analysis in this paper because reddening makes their true luminosity impossible to determine. They are included in Table 4 for completeness only.

Table 1. VLA observations.

Galaxy		Optical position (1950.0)	Radio position (1950.0)	Total flux density (mJy)	Size (arcsec)
NGC630	S0	01 33 25 −39 36 54		< 0.8	
NGC641	E	01 36 31 −42 46 48	01 36 30.8 −42 46 48	71.4	>60
NGC862	E-S0	02 11 02 −42 16 00	02 11 01.8 −42 15 54	1.1	<4.0
IC1795	S0	02 20 48 −41 35 54		< 0.8	
IC1864	E	02 51 37 −34 24 00	02 51 36.7 −34 24 02	0.9	<4.2
IC1875	E	03 02 02 −39 38 06		< 1.1	
NGC1316	S0	03 20 47 −37 23 12			>1°
IC1919	S0	03 24 02 −33 04 12		< 0.9	
NGC1336	S0	03 24 35 −35 53 18		< 0.7	
358-G06	E	03 25 20 −34 42 00		< 0.7	
NGC1351	S0	03 28 38 −35 01 24		< 0.8	
NGC1374	S0	03 33 21 −35 23 30		< 0.7	
NGC1375	S0	03 33 21 −35 25 54		< 0.7	
NGC1379	E	03 34 08 −35 36 18		< 0.8	
NGC1380	S0	03 34 32 −35 08 24	03 34 31.8 −35 08 25	1.7	<2.4
NGC1381	S0	03 34 36 −35 27 30		< 0.7	
NGC1380B	S0	03 35 13 −35 21 30		< 0.7	
NGC1389	S0	03 35 17 −35 54 30		< 1.0	
NGC1399	E	03 36 34 −35 36 42	03 36 34.1 −35 36 48	191.4	>240
NGC1404	E	03 36 57 −35 45 18		< 0.7	
NGC1411	S0	03 37 04 −44 15 42		< 0.8	
NGC1419	E	03 38 51 −37 40 18		< 0.7	
NGC1427	S0	03 40 25 −35 33 06		< 0.8	
NGC1428	S0	03 40 28 −35 18 42		< 0.7	
358-G59	E	03 43 10 −36 07 42		< 1.1	
IC2006	E-S0	03 52 36 −36 06 48		< 0.8	
IC2035	E	04 07 28 −45 38 54		< 0.7	
NGC1571	S0	04 20 33 −43 44 42		< 0.8	
NGC2310	S0	06 52 16 −40 47 54		< 0.8	
NGC2328	E-S0	07 01 01 −41 59 42	07 01 00.6 −41 59 39	2.5	< 2.5
367-G08	S0	07 14 50 −35 17 00		< 0.9	
NGC2663	E	08 43 08 −33 36 42	08 43 08.0 −33 36 43	750.0	>180
NGC3087	E	09 56 58 −33 59 06	09 56 57.8 −33 59 07	0.7	<18.2
IC2552	S0	10 08 34 −34 35 54		< 0.9	
NGC3224	E	10 19 27 −34 26 36		< 0.9	
NGC3250	E	10 24 21 −39 41 18		< 0.9	
NGC3258	E	10 26 39 −35 21 00	10 26 38.4 −35 20 54	18.3	45
NGC3268	E	10 27 45 −35 04 06	10 27 45.1 −35 04 06	22.8	< 5
NGC3271	S0	10 28 11 −35 06 06		< 1.0	
NGC3273	S0	10 28 14 −35 21 12		< 0.9	

Table 1 – *continued*

Galaxy		Optical position (1950.0)		Radio position (1950.0)		Total flux density (mJy)	Size (arcsec)
IC2587	S0	10 28 44	−34 18 24			< 0.9	
263-G48	S0	10 29 04	−45 59 36	10 29 04.5	−45 59 39	13.0	15
376-G07	E-S0	10 38 55	−36 53 00	10 38 55.0	−36 52 56	3.1	< 4.9
376-G09	S0	10 39 43	−32 59 00			< 0.8	
318-G21	E	10 50 48	−40 03 48	10 50 48.8	−40 03 47	1.5	< 3.8
NGC3557B	S0	11 07 10	−37 04 36	11 07 09.9	−37 04 32	0.8	< 7.4
NGC3557	E	11 07 35	−37 16 00	11 07 35.2	−37 16 03	217.8	>120
NGC3564	S0	11 08 14	−37 16 30			< 0.8	
NGC3573	S0	11 08 56	−36 36 06			< 0.9	
377-G29	S0	11 12 14	−33 38 00			< 0.8	
NGC3606	E-S0	11 13 51	−33 33 12			< 0.9	
378-G20	S0	11 44 46	−37 16 24			< 0.9	
NGC3706	S0	11 27 17	−36 07 00	11 27 19.7	−36 06 54	19.0	60
IC2977	S0	11 52 42	−37 25 00	11 52 42.3	−37 25 05	6.5	< 1.3
NGC4373	E-S0	12 22 39	−39 29 00	12 22 38.3	−39 28 59	12.7	< 1.3
322-G08	S0	12 22 58	−39 02 36	12 22 58.4	−39 02 35	3.2	< 2.8
IC3370	E	12 24 57	−39 03 42	12 24 57.4	−39 03 40	6.4	< 1.6
322-G51	S0	12 38 10	−41 19 54			< 1.0	
NGC4645A	S0	12 40 21	−41 05 06			< 7.5	
NGC4696	S0	12 46 04	−41 02 18	12 46 03.5	−41 02 19	1227.0	45
NGC4709	S0	12 47 18	−41 06 36			< 1.2	
323-G16	E-S0	12 49 00	−40 51 36			< 0.8	
323-G19	E-S0	12 49 17	−41 11 18			< 0.8	
NGC4743	S0	12 49 29	−41 07 06			< 0.9	
NGC4751	S0	12 50 04	−42 23 18	12 50 03.4	−42 23 19	3.0	< 3.1
323-G34	E	12 50 39	−40 56 00			< 0.9	
NGC4767	E	12 51 07	−39 26 36			< 0.9	
269-G08	S0	12 52 34	−44 32 36	12 52 34.0	−44 32 31	1.0	< 4.6
381-G29	E	12 53 43	−36 06 00	12 53 42.8	−36 06 02	3.5	< 1.6
NGC4832	S0	12 55 00	−39 29 24			< 0.9	
NGC4946	S0	13 02 38	−43 19 24			< 0.8	
323-G92	E	13 09 25	−39 40 24			< 0.9	
NGC5011	S0	13 09 59	−42 49 54			< 0.8	
323-G93	S0	13 10 22	−42 01 18	13 10 21.6	−42 01 18	20.5	< 1
382-G34	S0	13 15 12	−36 41 12			< 0.8	
NGC5062	S0	13 15 34	−35 11 42	13 15 34.3	−35 11 44	0.9	< 4.8
NGC5090A	S0	13 16 26	−43 23 12	13 16 26.3	−43 23 13	1.2	< 4.9
NGC5090	E	13 18 18	−43 26 36			779.6	>360
NGC5102	S0	13 19 07	−36 22 12			< 0.8	
NGC5128	E	13 22 33	−42 45 24				>1°
NGC5140	S0	13 23 31	−33 36 30	13 23 31.8	−33 36 30	29.2	< 5
NGC5193	E	13 29 03	−32 58 42			< 0.8	
NGC5220	S0	13 33 05	−33 11 54			< 0.8	
IC4296	E	13 33 47	−33 42 42	13 33 47.1	−33 42 41	511.0	>120
NGC5237	S0	13 34 40	−42 35 36			< 0.9	
383-G45	S0	13 34 47	−33 33 30	13 34 47.5	−33 33 26	2.6	< 1.3
384-G13	S0	13 52 47	−33 28 54			< 0.8	
384-G19	S0	13 54 44	−33 58 30			< 0.9	
NGC5397	S0	13 58 14	−33 42 12			< 0.8	
NGC5419	S0	14 00 42	−33 44 18	14 00 42.2	−33 44 20	129.4	>30

Table 1 – *continued*

Galaxy		Optical position (1950.0)		Radio position (1950.0)		Total flux density (mJy)	Size (arcsec)
IC4421	E	14 25 27	−37 21 36			< 0.9	
IC4451	E	14 31 33	−36 04 00			< 0.9	
NGC5670	S0	14 32 30	−45 44 54			< 1.5	
IC4464	E-S0	14 34 44	−36 39 42			< 0.8	
337-G10	S0	19 02 27	−42 26 36	19 02 27.5	−42 26 32	4.5	< 1.5
NGC6768	S0	19 13 05	−40 17 54	19 13 05.3	−40 17 54	2.5	< 2.5
IC4931	S0	19 57 30	−38 42 48	19 57 30.3	−38 42 48	0.9	< 4.3
NGC6849	E	20 02 54	−40 20 30			< 0.7	
IC4956	S0	20 07 59	−45 44 30	20 07 59.7	−45 44 31	6.1	< 2.6
IC4991	S0	20 15 01	−41 12 24	20 15 01.3	−41 12 23	4.7	60
IC5011	S0	20 25 21	−36 11 36	20 25 21.0	−36 11 37	0.8	< 2.3
NGC6958	E	20 45 30	−38 10 54	20 45 29.8	−38 10 58	18.1	< 0.5
286-G50	E	21 03 25	−42 45 24			< 1.2	
342-G27	S0	21 13 41	−42 28 06			< 0.7	
IC5105	E-S0	21 21 12	−40 45 06	21 21 11.9	−40 45 11	3.7	< 3.0
NGC7057	S0	21 21 46	−42 40 36			< 0.8	
NGC7070A	S0	21 28 36	−43 04 00	21 28 35.5	−43 04 06	1.3	< 3.0
NGC7079	S0	21 29 22	−44 17 18			< 0.8	
NGC7097	E	21 37 04	−42 46 00	21 37 03.5	−42 45 59	17.5	< 1.3
NGC7166	S0	21 57 27	−43 37 48	21 57 26.7	−43 37 46	0.6	< 4.6
IC5157	E-S0	22 00 30	−35 11 00	22 00 30.2	−35 11 03	1.1	< 2.9
NGC7404	E-S0	22 51 29	−39 34 54			< 0.7	
IC5267B	S0	22 54 05	−44 01 42			< 0.7	
IC1459	E	22 54 23	−36 43 48	22 54 23.1	−36 43 47	1016.1	< 1.0
IC5269	S0	22 54 57	−36 17 36	22 54 58.1	−36 17 06	3.1	< 1.5
NGC7484	S0	23 04 19	−36 32 41	23 04 19.6	−36 32 45	2.7	< 0.8

NGC 3250: This galaxy was detected at Parkes, but there is no sign of a source on the VLA map. The Parkes detection may be spurious, or this could be a weak extended source without a high surface brightness central component, which might also account for the very steep spectral index of −1.7 measured at Parkes. For now, it is treated as a non-detection in the VLA sample.

NGC 3706: The VLA map shows an unusual structure (Fig. 1e), with a central source of 7.6 mJy and extended emission to the south-east of the nucleus. The galaxy was also detected at Parkes at 6 cm by Disney & Wall (1977), and at 2 cm by Ekers *et al.* (1980, private communication) with flux densities of 21 mJy and 13 mJy respectively. We have assumed that all the emission is associated with the galaxy, giving a 6-cm flux density of 19.0 mJy at the VLA, and a spectral index of −0.3.

2.3 STRUCTURE OF THE EXTENDED RADIO SOURCES

Fourteen of the 49 galaxies detected at the VLA have extended radio emission, on scales from 15 arcsec to several degrees. Maps of seven of these sources are shown in Fig. 1. Of the remainder, two (ESO 263-G48 and NGC 4696) belong to the dust-lane galaxy sample observed by Laing *et al.* (1989, in preparation) while for the others (NGC 1316, 1399, 5090, 5128 and IC 4296), existing maps by other observers show more detail than is visible in our VLA snapshots. References to these maps are given in Table 2.

Table 3 lists optical and radio position angles for the extended radio sources. The optical values are from the ESO/Uppsala catalogue (Lauberts 1982), except for NGC 1399, NGC 5419 (Sansom *et al.* 1987), IC 4296 (Killeen, Bicknell & Ekers 1986) and NGC 5090

Table 2. Core components of galaxies with extended radio emission.

Galaxy	Type	Flux (mJy)	Size (arcsec)	S_{core}/S_{tot}	Ref.	Map
NGC641	E	10	< 2.5	0.10	1	1
NGC1316	E	26	< 0.5	0.0004	2	4
NGC1399	E	10	< 0.4	0.03	2	5
NGC2663	E	160	< 3.7	0.15	1	1,6
NGC3258	E	3.7	< 5	0.07	1	1
263-G48	S0	1.5	< 1.0	0.08	1	7
NGC3557	E	10	< 0.4	0.03	2	1,4
NGC3706	S0	7.6	< 5	0.40	1	1,8
NGC4696	E	55	< 1.3	0.04	1	7
NGC5090	E	268	< 10	0.16	1	9
NGC5128	E	6984	< 3	0.11	3	10
IC4296	E	218	< 3	0.14	1	11
		210	< 0.4		2	
NGC5419	S0	15	< 0.3	0.10	2	1
IC4991	S0	1.4	< 4.0	0.07	1	1

Column 6 lists the source of each measurement, while column 7 gives references to published radio maps. The coding for columns 6 and 7 is as follows: (1) this survey, (2) Ekers *et al.* (1989), (3) Burns, Feigelson & Schreier (1983), (4) Birkinshaw & Davies (1985), (5) Killeen, Bicknell & Ekers (1988), (6) Danziger & Goss (1983), (7) Laing *et al.* (1989; in preparation), (8) Wilkinson *et al.* (1987), (9) Smith & Bicknell (1986), (10) Haynes, Cannon & Ekers (1983), (11) Killeen *et al.* (1986).

Table 3. Optical and radio position angles for galaxies with extended radio emission.

Galaxy	Position angle (deg.) Optical	Radio	Axial ratio log(a/b)
NGC641	–	35	0.000
NGC1316	50	147	0.054
NGC1399	112	171	0.000
NGC2663	110	159	0.204
NGC3258	75	22	0.054
263-G48	168	100	0.329
NGC3557	30	79	0.109
NGC3706	78	118	0.279
NGC4696	95	100	0.125
NGC5090	98	36	0.000
NGC5128	35	35	0.115
IC4296	61	131	0.000
NGC5419	90	176	0.067
IC4991	145	170	0.194

(White, McAdam & Jones 1984). NGC 641 is a round galaxy which appears to have no reliably determined optical position angle. Although there is no clearly-preferred orientation for the extended radio emission, the separation of radio axis and optical minor axis is between 0° and 50° for 10 of the 13 galaxies with reliably measured position angles, in agreement with the result found by Birkinshaw & Davies (1985) for a larger sample of extended sources.

2.4 BACKGROUND SOURCE DENSITY AND CONFUSION AT 5 GHz

The VLA survey maps showed many background sources with flux density 1–25 mJy. Taking only the central 4.4 arcmin of each field (corresponding to the half-power level of the primary

Table 4. Optical, radio and [N II] emission-line luminosities for the PKS/VLA galaxy sample.

Galaxy	Type	Dist. (Mpc)	M_B (mag.)	log F (W)	log P (W/Hz)	log(a/b)	
149-G19	E-S0	93.2	−21.3		23.3	0.380	V
194-G21	S0	32.2	−19.5		< 21.4	0.079	V
NGC312	E	77.9	−21.3		< 22.4	0.062	P
NGC323	E	77.4	−21.3		< 22.2	0.079	P
151-G12	S0	73.1	−20.9		< 22.2	0.250	P
IC1625	E-S0	65.5	−21.2	32.8	< 21.9	0.051	P
013-G12	S0	48.4	−20.8	< 32.0	22.4	0.628	P
IC1633	S0	71.2	−22.0		< 22.0	0.016	P
NGC484	S0	50.6	−20.9	32.9	< 22.0	0.125	P
NGC630	S0	58.2	−20.6	32.6	< 20.5	0.000	V
NGC641	E	61.9	−21.2		22.7	0.000	V
244-G45	E-S0	63.3	−20.6		< 22.1	0.000	P
NGC745	E	58.1	−20.4	32.0	< 21.9	0.176	P
NGC802	E-S0	13.2	−16.9	30.8	< 20.6	0.176	P
NGC862	E-S0	51.6	−20.2	31.8	20.5	0.000	V
IC1796	S0	49.6	−19.8	32.7	< 20.4	0.097	V
IC1864	E	44.1	−20.0	32.7	20.3	0.243	V
IC1875	E	59.6	−20.4	< 32.1	< 20.7	0.000	V
NGC1316	S0	16.3	−21.7		24.3	0.054	V
IC1919	S0	11.8	−17.0	< 31.3	< 19.2	0.163	V
NGC1336	S0	11.8	−17.3	< 30.8	< 19.1	0.109	V
358-G06	E	11.0	−16.5	< 31.3	< 19.0	0.301	V
NGC1351	S0	13.5	−18.3	< 31.3	< 19.2	0.301	V
NGC1374	S0	11.1	−18.4		< 19.0	0.061	V
NGC1375	S0	5.2	−16.0	< 30.2	< 18.4	0.439	V
NGC1379	E	12.2	−19.0		< 19.2	0.000	V
NGC1380	S0	16.6	−20.2	31.9	19.7	0.252	V
NGC1381	S0	16.3	−18.9		< 19.3	0.588	V
NGC1380B	S0	17.8	−17.7		< 19.4	0.000	V
NGC1389	S0	9.3	−17.7		< 19.0	0.211	V
NGC1399	E	13.0	−20.2		21.8	0.000	V
NGC1404	E	18.6	−20.6		< 19.5	0.028	V
NGC1411	S0	7.9	−17.5	31.2	< 18.8	0.143	V
NGC1419	E	13.7	−17.4		< 19.2	0.000	V
NGC1427	S0	14.2	−19.1		< 19.3	0.194	V
NGC1428	S0	14.9	−18.2		< 19.3	0.331	V
358-G59	E	8.7	−15.9		< 19.0	0.176	V
IC2006	E-S0	12.3	−18.3		< 19.2	0.075	V
NGC1490	E	51.8	−20.4		< 21.8	0.138	P
IC2035	E	12.6	−18.5		< 19.1	0.138	V
NGC1533	S0	5.6	−17.1	31.1	< 20.1	0.067	P
NGC1549	E-S0	9.8	−19.4	< 31.0	< 20.5	0.109	P
NGC1553	S0	10.2	−20.0	32.0	< 20.6	0.273	P
NGC1567	S0	43.5	−20.3		< 22.7	0.000	P
NGC1571	S0	41.5	−20.2		< 20.2	0.079	V
NGC1574	S0	6.7	−17.9		< 20.2	0.051	P
NGC1596	S0	12.5	−18.9		< 20.8	0.643	P
NGC1595	E	44.7	−19.8	< 32.9	< 21.9	0.160	P
118-G34	S0	9.5	−16.7	32.2	< 20.3	0.046	P
NGC1705	S0	4.0	−15.4	29.2	< 19.9	0.151	P
NGC1930	E	40.5	−20.4		< 21.8	0.155	P
NGC1947	S0	9.7	−18.5		20.3	0.000	P
NGC2191	S0	41.9	−20.4		< 21.6	0.376	P
NGC2305	E	32.5	−20.4		< 21.6	0.079	P
NGC2310	S0	9.5	−17.7		< 18.9	0.720	V
NGC2328	E-S0	8.8	−17.0	32.4	19.4	0.058	V
367-G08	S0	26.5	−19.4	32.2	< 19.9	0.248	V
IC2200A	S0	29.6	−19.2	< 33.0	< 21.3	0.211	P
208-G21	E	8.1	−18.1	31.9	< 20.2	0.097	P
NGC2434	S0	12.0	−18.8	< 32.2	< 20.5	0.028	P

Table 4 – *continued*

Galaxy	Type	Dist. (Mpc)	M_B (mag.)	log F (W)	log P (W/Hz)	log(a/b)	
NGC2502	E-S0	7.1	−17.2	31.3	< 19.6	0.301	P
NGC2640	S0	7.5	−18.8	32.4	20.3	0.067	P
NGC2663	E	18.4	−21.0	32.5	22.6	0.204	V
NGC2887	E	26.5	−21.1	< 33.2	< 21.3	0.176	P
NGC3087	E	23.9	−19.9	< 32.8	19.7	0.046	V
NGC3136	E	14.1	−20.9	32.8	< 20.7	0.176	P
IC2552	S0	27.2	−19.6	< 32.0	< 19.9	0.000	V
NGC3136B	E	15.0	−19.6	< 32.5	< 21.0	0.301	P
NGC3224	E	26.8	−19.7	< 32.0	< 19.9	0.067	V
NGC3250	E	25.5	−20.5	< 32.2	< 19.8	0.125	V
NGC3258	E	25.3	−19.8	< 32.3	21.6	0.054	V
NGC3260	E	21.3	−18.0	31.9	< 21.3	0.125	P
NGC3268	E	25.2	−19.7	32.2	21.3	0.138	V
NGC3271	S0	35.0	−20.7	< 32.4	< 20.2	0.352	V
NGC3273	S0	21.4	−18.7		< 19.7	0.398	V
IC2587	S0	18.6	−18.3		< 19.6	0.079	V
263-G48	S0	26.0	−20.4	< 32.7	21.2	0.329	V
376-G07	E-S0	40.4	−19.6		20.8	0.281	V
376-G09	S0	27.5	−19.2		< 19.9	0.677	V
318-G21	E	45.5	−20.2		20.6	0.204	V
NGC3557B	S0	25.7	−19.4	< 31.0	19.8	0.615	V
NGC3557	E	26.7	−21.1		22.4	0.109	V
NGC3564	S0	25.0	−19.3		< 19.8	0.243	V
NGC3573	S0	20.9	−19.2		< 19.7	0.609	V
377-G29	S0	24.0	−18.7		< 19.7	0.452	V
NGC3606	E-S0	27.5	−18.7		< 19.9	0.000	V
NGC3706	S0	27.8	−20.3		21.2	0.279	V
378-G20	S0	27.7	−19.1		< 19.9	0.385	V
IC2977	S0	27.7	−19.7		20.8	0.301	V
NGC4373	E-S0	31.7	−21.0		21.2	0.079	V
322-G08	S0	26.9	−19.3		20.4	0.465	V
IC3370	E	26.8	−20.6		20.7	0.079	V
NGC4601	S0	2.0	−12.5		< 20.1	0.501	P
322-G51	S0	30.2	−19.0		< 20.0	0.602	V
NGC4645A	S0	29.4	−19.6		< 20.9	0.544	V
NGC4645B	S0	23.2	−18.9	< 31.4	< 20.7	0.495	P
381-G12	S0	57.0	−20.8	32.4	< 21.9	0.046	P
NGC4645	E	24.1	−19.4	31.6	< 21.3	0.222	P
NGC4696B	S0	29.4	−19.1	32.0	< 21.5	0.192	P
NGC4696	S0	26.1	−21.0	31.9	23.1	0.125	V
322-G102	S0	35.1	−19.4		< 21.8	0.753	P
NGC4706	S0	34.4	−19.4		< 21.6	0.426	P
NGC4709	S0	43.9	−20.8		< 20.4	0.046	V
323-G16	E-S0	19.9	−18.3		< 19.6	0.000	V
323-G19	E-S0	35.1	−19.3		< 20.1	0.359	V
NGC4743	S0	27.8	−19.1		< 19.9	0.426	V
NGC4751	S0	16.8	−18.7		20.0	0.368	V
323-G34	E	40.0	−21.0		< 20.2	0.301	V
NGC4767	E	27.5	−20.1		< 19.9	0.363	V
269-G08	S0	68.2	−20.8		20.7	0.051	V
381-G29	E	24.0	−18.8	32.6	20.4	0.301	V
IC3896	S0	20.3	−19.7	< 32.3	< 21.0	0.143	P
NGC4832	S0	35.2	−20.0	< 32.4	< 20.1	0.204	V
NGC4940	S0	49.0	−20.3	32.7	< 22.2	0.041	P
NGC4946	S0	29.0	−19.4		< 19.9	0.260	V
NGC4976	S0	11.3	−19.8	< 32.4	< 20.7	0.234	P
269-G58	S0	16.2	−18.8	31.2	< 21.0	0.176	P
323-G92	E	30.0	−19.5	< 32.3	< 20.0	0.125	V
NGC5011	S0	28.8	−20.2	32.2	< 19.9	0.049	V
323-G93	S0	32.3	−19.9	< 33.4	21.6	0.230	V

Table 4 – *continued*

Galaxy	Type	Dist. (Mpc)	M_B (mag.)	log F (W)	log P (W/Hz)	log(a/b)	
382-G34	S0	29.6	−19.0		< 19.9	0.035	V
NGC5062	S0	31.0	−19.7		20.0	0.501	V
269-G80	S0	29.7	−19.2		< 21.5	0.030	P
NGC5090A	S0	32.0	−19.7		20.2	0.419	V
269-G90	S0	29.2	−19.3		< 21.3	0.301	P
NGC5090	E	32.0	−19.9	32.6	23.3	0.000	V
NGC5102	S0	2.5	−16.5	< 29.8	< 18.4	0.362	V
NGC5128	E	5.0	−21.1		23.3	0.115	V
NGC5140	S0	36.8	−20.5	32.2	21.8	0.046	V
NGC5193	E	35.3	−20.5	31.9	< 20.1	0.000	V
NGC5206	S0	3.6	−15.4	< 30.0	< 20.0	0.079	P
NGC5220	S0	39.9	−20.1	32.2	< 20.2	0.477	V
IC4296	E	34.4	−21.3	32.2	23.4	0.000	V
NGC5237	S0	2.0	−13.9	28.5	< 18.4	0.075	V
383-G45	S0	37.3	−19.4	32.6	20.6	0.477	V
383-G49	S0	36.7	−19.0	< 32.2	< 21.8	0.380	P
NGC5266	S0	28.3	−20.4	32.7	< 21.5	0.146	P
NGC5333	S0	25.4	−20.0	32.0	< 21.3	0.301	P
384-G13	S0	35.1	−19.2	32.0	< 20.1	0.105	V
384-G19	S0	40.3	−19.6	32.1	< 20.2	0.097	V
NGC5397	S0	39.5	−19.6	32.0	< 20.2	0.250	V
NGC5419	S0	39.1	−21.2	< 32.2	22.4	0.067	V
221-G26	E-S0	12.3	−19.0	< 30.2	< 20.7	0.176	P
IC4421	E	34.5	−19.4	31.8	< 20.1	0.176	V
IC4451	E	38.0	−20.6	< 31.7	< 20.2	0.117	V
NGC5670	S0	27.4	−20.1	31.4	< 20.1	0.368	V
IC4464	E-S0	41.1	−20.0	32.2	< 20.2	0.456	V
NGC5799	S0	28.5	−20.4		< 21.4	0.176	P
*137-G08	S0	38.6	−22.4		< 24.2		P
*137-G10	E-S0	32.1	−21.3		< 23.4		P
101-G14	S0	23.1	−19.7	32.2	< 21.1	0.035	P
137-G45	E	32.0	−20.3	< 32.6	21.6	0.155	P
069-G14	S0	45.4	−21.0	< 32.7	< 21.7	0.176	P
138-G05	S0	26.9	−20.5	32.7	< 21.2	0.117	P
NGC6305	S0	26.3	−20.6	< 31.0	< 21.3	0.222	P
NGC6407	S0	44.9	−21.3	< 32.0	< 21.8	0.125	P
NGC6483	E	47.8	−21.0	< 31.7	< 21.8	0.301	P
NGC6438	E-S0	22.3	−19.4	< 31.1	< 21.2	0.079	P
182-G07	E	49.0	−20.5	< 31.8	< 22.1	0.447	P
IC4704	S0	33.8	−20.2	< 31.4	< 21.7	0.073	P
NGC6653	S0	49.9	−20.7	< 33.0	< 21.8	0.035	P
NGC6673	S0	10.0	−18.3	< 31.8	< 20.6	0.398	P
IC4765	S0	44.2	−21.3	< 32.6	< 21.8	0.222	P
104-G07	E-S0	37.5	−19.7	< 32.6	< 21.7	0.301	P
IC4797	S0	26.5	−20.5	< 32.8	< 21.2	0.357	P
183-G30	S0	26.4	−20.2	< 31.7	< 21.2	0.079	P
NGC6721	S0	43.1	−20.7	31.8	< 21.9	0.067	P
NGC6725	S0	35.2	−20.5	< 31.1	< 21.5	0.643	P
NGC6733	S0	47.8	−20.6	< 31.5	< 22.0	0.103	P
NGC6730	E	41.4	−20.4	31.7	22.2	0.038	P
337-G10	S0	58.2	−21.0	32.3	21.3	0.000	V
NGC6739	S0	41.6	−20.7	32.1	< 21.8	0.398	P
NGC6746	S0	40.4	−19.9	31.9	< 21.6	0.273	P
184-G33	S0	39.5	−19.8	32.3	< 21.6	0.038	P
NGC6758	E	33.1	−20.7	32.8	21.6	0.158	P
NGC6768	S0	55.6	−20.9	< 32.7	21.0	0.000	V
NGC6771	S0	41.1	−20.5	32.5	< 21.6	0.716	P
NGC6776	S0	53.3	−21.5	33.1	< 22.0	0.067	P
105-G04	E-S0	38.1	−19.6	< 32.4	< 21.6	0.146	P
NGC6799	S0	55.1	−20.7	< 32.7	< 21.9	0.133	P
142-G19	S0	41.2	−20.2	< 32.6	< 21.6	0.661	P
232-G21	S0	39.3	−19.4	32.2	21.8	0.778	P
IC4889	E	24.7	−20.3	32.5	< 21.2	0.255	P
IC4906	S0	36.8	−19.7	32.4	< 21.5	0.250	P

Table 4 – *continued*

Galaxy	Type	Dist. (Mpc)	M_B (mag.)	log F (W)	log P (W/Hz)	log(a/b)	
IC4931	S0	59.3	−21.3	< 32.7	20.6	0.000	V
NGC6848	S0	42.2	−20.9	32.1	< 21.8	0.491	P
185-G54	S0	42.9	−20.8	< 31.7	< 21.8	0.163	P
NGC6851	S0	29.9	−20.4	32.4	< 21.3	0.125	P
NGC6854	S0	56.1	−21.3		< 21.9	0.046	P
IC4943	E	27.1	−18.8		< 21.4	0.204	P
NGC6849	E	59.5	−21.1	< 32.9	< 20.5	0.000	V
NGC6861	E	27.8	−20.6	32.8	21.3	0.252	P
NGC6861D	S0	24.5	−19.2	32.3	< 21.2	0.459	P
NGC6868	E	28.5	−21.1	33.1	22.1	0.135	P
IC4956	S0	51.2	−20.9	33.1	21.3	0.000	V
NGC6875	S0	30.8	−19.9		< 21.6	0.301	P
NGC6876	S0	57.6	−21.1	32.1	< 21.5	0.079	P
NGC6877	E-S0	39.8	−20.0	32.3	< 21.8	0.398	P
NGC6880	S0	37.8	−19.5	32.5	< 21.5	0.186	P
IC4991	S0	57.9	−21.7	< 32.6	21.9	0.194	V
186-G36	S0	45.9	−20.3	< 32.3	< 21.9	0.523	P
234-G21	S0	53.5	−20.5	33.7	< 21.9	0.135	P
NGC6909	E	27.1	−20.1	< 32.5	< 21.2	0.363	P
IC5011	S0	23.1	−19.5	< 32.6	19.7	0.279	V
NGC6920	S0	25.9	−19.1	32.2	< 21.2	0.051	P
NGC6958	E	27.1	−20.2	32.9	21.4	0.097	V
NGC6987	E-S0	52.8	−20.5	33.1	22.3	0.000	P
107-G04	E	31.9	−20.1	< 32.6	< 22.2	0.138	P
235-G42	S0	48.6	−19.8	32.2	< 21.8	0.155	P
NGC7002	E	74.4	−21.6	< 32.8	22.5	0.067	P
235-G49	E	47.8	−20.3	32.8	< 21.8	0.204	P
NGC7007	S0	29.0	−19.8	32.3	< 21.4	0.186	P
286-G49	E	51.4	−19.9	32.9	< 21.9	0.204	P
286-G50	E	26.3	−18.9	< 31.9	< 20.0	0.301	V
NGC7014	E-S0	47.2	−20.4	< 32.7	< 21.8	0.176	P
NGC7029	E	27.8	−20.1	< 30.7	< 21.4	0.155	P
NGC7041	S0	18.4	−19.5	< 31.5	< 20.9	0.456	P
342-G27	S0	52.6	−20.6	31.5	< 20.4	0.125	V
235-G85	E	22.4	−18.1	< 31.1	< 21.1	0.301	P
NGC7049	S0	21.9	−20.3	32.0	21.3	0.301	P
IC5105	E-S0	53.9	−21.2		21.1	0.176	V
NGC7057	S0	51.1	−20.6	< 31.3	< 20.4	0.230	V
011-G03	S0	23.3	−18.2	31.4	< 21.2	0.263	P
NGC7070A	S0	23.6	−19.1	31.2	19.9	0.000	V
NGC7079	S0	26.6	−20.2		< 19.8	0.125	V
NGC7097	E	26.0	−19.8		21.2	0.125	V
NGC7117	E-S0	55.2	−20.2	31.6	< 22.0	0.243	P
NGC7118	E-S0	51.1	−20.2	31.9	< 22.0	0.135	P
NGC7123	S0	36.3	−20.0	31.1	< 21.5	0.398	P
NGC7144	S0	18.9	−19.9	< 31.4	< 20.9	0.000	P
NGC7145	S0	18.7	−19.6		< 20.9	0.000	P
NGC7166	S0	24.0	−19.4	31.3	19.6	0.374	V
NGC7168	E-S0	27.1	−19.5	< 31.4	< 21.5	0.176	P
IC5157	E-S0	44.9	−19.4	31.8	20.4	0.000	V
NGC7196	E	28.9	−20.3		< 21.0	0.071	P
NGC7192	E	27.6	−20.1		< 21.1	0.000	P
NGC7200	E-S0	28.4	−18.8	31.4	< 21.3	0.073	P
NGC7213	S0	17.6	−20.5	32.1	21.9	0.000	P
NGC7216	E	33.2	−19.5	32.2	21.8	0.336	P
IC5181	S0	20.4	−19.5		< 21.1	0.447	P
NGC7404	E-S0	19.9	−18.3	< 31.7	< 19.5	0.263	V
IC5267B	S0	16.1	−18.1	< 30.1	< 19.3	0.385	V
IC1459	E	17.0	−20.5	32.7	22.6	0.155	V
IC5269	S0	21.3	−18.9	< 31.8	20.2	0.301	V
027-G21	S0	23.1	−18.5	32.0	< 21.3	0.090	P
NGC7484	S0	27.5	−19.8	< 32.2	20.4	0.000	V
NGC7676	E	31.9	−19.5	< 32.4	< 21.6	0.368	P
NGC7796	E	32.2	−20.3	< 32.6	< 21.4	0.000	P

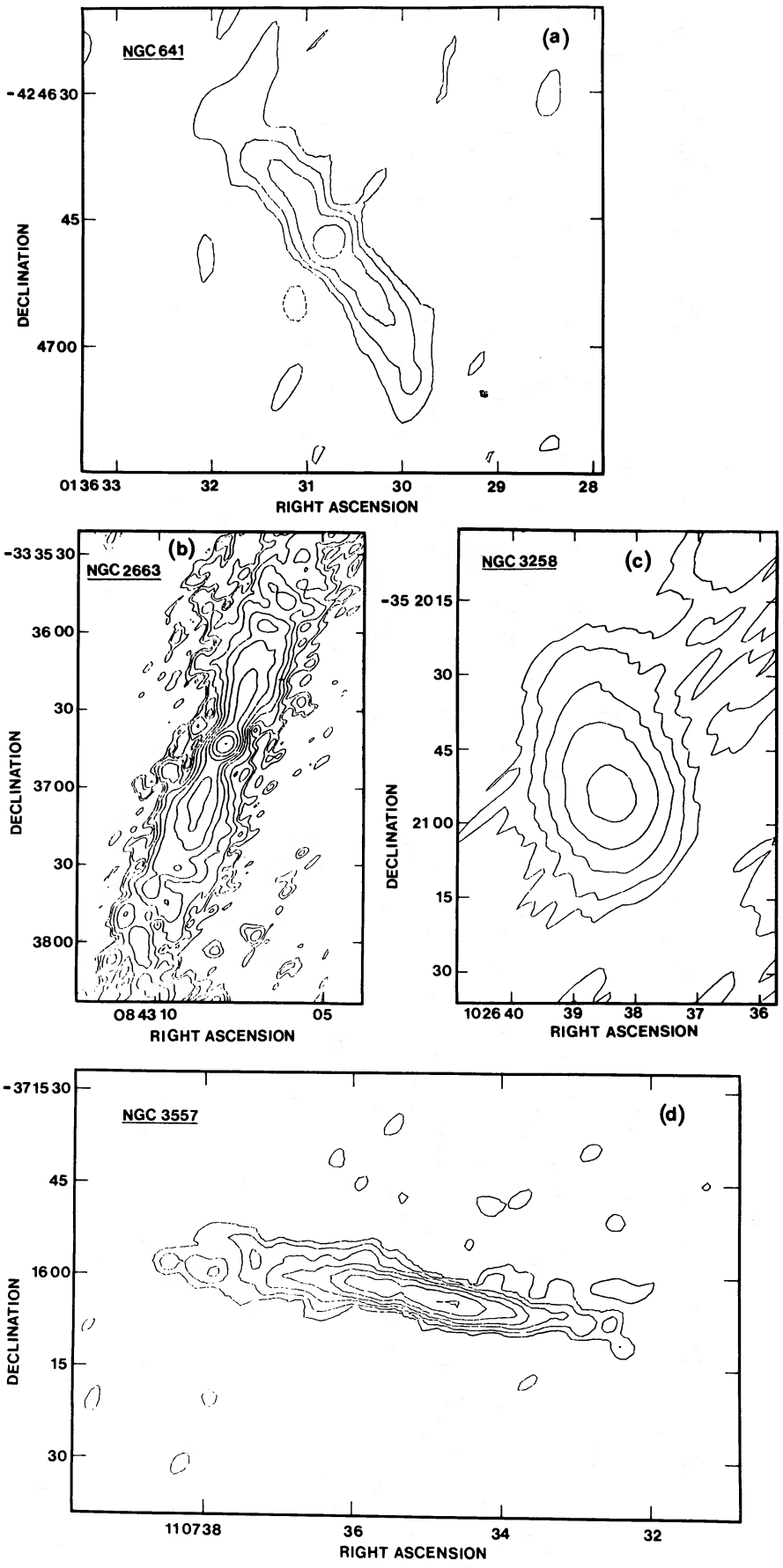

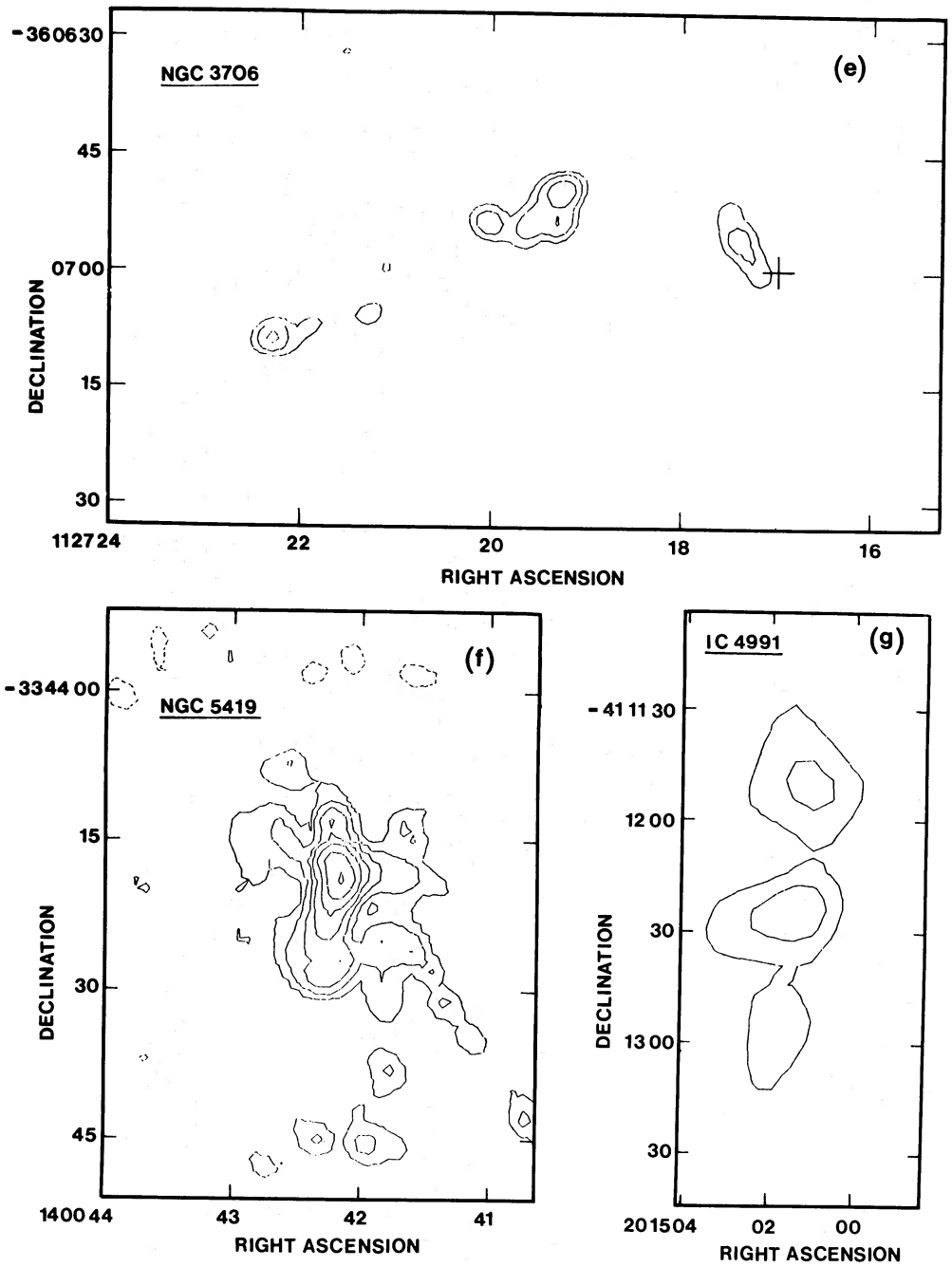

Figure 1. VLA 5-GHz continuum maps for the following galaxies: (a) NGC 641 – contour levels −0.3, 0.3, 0.6, 1.2, 2.4 mJy; (b) NGC 2663 – contour levels 0.3, 0.6, 1.2, 2.4, 4.8, 9.6, 19.2, 38.4, 76.8, 153.6 mJy; (c) NGC 3258 – contour levels 0.3, 0.6, 1.2, 2.4, 4.8 mJy; (d) NGC 3557 – contour levels 0.3, 0.6, 1.2, 2.4, 4.8, 9.6, 19.2 mJy; (e) NGC 3706 – contour levels 0.3, 0.6, 1.2 mJy (the optical centre of the galaxy is marked by a cross); (f) NGC 5419 – contour levels −0.4, 0.4, 0.8, 1.6, 3.2, 6.4, 12.8, 25.6 mJy; (g) IC 4991 – contour levels 0.5, 1.0 mJy.

beam), the total area of sky covered by the 109 fields surveyed at the VLA is 5.62×10^{-4} sr (1.84 square degrees). Within this area are 58 background sources in the range 1–10 mJy and a further nine sources above 10 mJy. This gives a number density $\log N = 5.076\ (\pm 0.05)\ \mathrm{sr}^{-1}$ for background sources above 1 mJy, in good agreement with the value of $\log N = 5.117\ \mathrm{sr}^{-1}$ found from the intermediate field survey by Fomalont *et al.* (1984). Our survey covers 10 times the area of the intermediate fields.

Using our derived value of $\log N$, the probability that a background source of flux density ≥ 1 mJy lies within 10 arcsec of the nucleus of one of our program galaxies is less than 0.1 per cent. Confusion is therefore unimportant in the present survey. We can also estimate the effects of confusion at lower flux limits. If we assume

$$N(S > S_0) \propto S^{\gamma}, \qquad \text{with } \gamma \simeq -1.5,$$

(Wall, Shimmins & Merkelijn 1971), the *a priori* probability of a 0.1 mJy source within 10 arcsec of the nucleus of any particular galaxy is about 3 per cent. Confusion is therefore unlikely to be a serious problem for surveys at flux levels 10 times lower than those measured here.

3 The local radio luminosity function

3.1 THE COMBINED GALAXY SAMPLE

Since the observations described here were made on a galaxy sample with well-defined selection criteria, they can be used to determine the local space density of radio galaxies. The only previous determination of the radio luminosity function at 5 GHz was by Ekers & Ekers (1973), using 11 detected galaxies.

In calculating the luminosity function, galaxies detected at 5 GHz in the VLA and Parkes surveys were combined with radio galaxies from the Wall & Peacock (1985; hereafter WP) all-sky catalogue (which also has well-defined selection criteria) in order to cover as large a range in radio power as possible. Although the original WP sample is radio-selected, we restrict ourselves to those sources identified as galaxies within a certain redshift limit. Thus, provided the selection criteria are rigidly specified, we can validly combine this sample with our own radio survey of optically selected galaxies to derive the radio luminosity function. The selection criteria applied were as follows:

From the Wall & Peacock catalogue,

(i) $z < 0.1$ (so evolutionary effects can be neglected);
(ii) $S_{2.7} \geq 2.4$ Jy;
(iii) source identified as a galaxy.

Although the WP catalogue aims to include all sources above 2.0 Jy at 2.7 GHz, the $V/V_{\max}$ test (Schmidt 1968) suggests some incompleteness below 2.4 Jy ($\langle V/V_{\max} \rangle = 0.466 \pm 0.017$ at 2.0 Jy and 0.493 ± 0.019 at 2.4 Jy), so we used 2.4 Jy as the flux limit.

Several nearby (spiral) Seyfert galaxies were removed from the WP sample, since we are considering only early-type galaxies, but the radio luminosity function of Seyferts (Meurs & Wilson 1984) suggests that spirals are unlikely to appear in the WP sample at larger redshifts. The final WP sample comprised 55 galaxies.

For the Parkes and VLA samples (based on optically selected E and S0 galaxies), the criteria are:

(i) $B_T \leq 13.6$;
(ii) south of $-32.5°$ declination;
(iii) $S_{2.7} > 40$ mJy at Parkes or $S_5 > 0.8$ mJy at the VLA.

Again, the final selection criteria were those for which a V/V_{max} test showed that the resulting sample was complete ($\langle V/V_{max}\rangle = 0.50 \pm 1/\sqrt{12N}$), so a few detected galaxies were excluded from the calculation. The combined PKS and VLA samples contain 45 detected galaxies which fulfil the selection criteria, but there is some overlap with the WP sample, so the methods described by Avni & Bahcall (1980) were used to produce three independent samples containing 97 objects with (total) radio powers ranging from $10^{19.4}$ to $10^{25.8}$ W Hz^{-1}. The samples cover 7.745 sr (WP), 1.269 sr (PKS) and 0.796 sr (VLA), and exclude regions within 10° of the galactic plane.

Table 5 lists some corrected fluxes for Parkes detections south of −45° (Sadler 1984c), based on recent maps (J. Harnett, private communication) from the Molonglo Observatory Synthesis Telescope (MOST; Mills 1981). These values were adopted in place of the earlier ones in all calculations.

3.2 DERIVATION OF THE RADIO LUMINOSITY FUNCTION (RLF)

The V/V_{max} method described by Schmidt (1968) was used to calculate the radio luminosity function (RLF), $\Phi(P)$ listed in Table 6. Following Schmidt & Green (1986), and with $q_0 = 1/2$, the bolometric luminosity distance of each galaxy is

$$A(t) = (2c/H_0)\, t(t-1), \qquad \text{where } t = (1+z)^{1/2}$$

and the comoving volume element is

$$V(t) = WA^3/t^6$$

for a survey area of W steradians. Bins of 1 dex were used in the calculation, but the result is quoted in galaxies mag^{-1} Mpc^{-3} (1 mag = 0.4 dex) for comparison with other published values. Fig. 2 shows the RLF at 5 GHz. Previous derivations at 1.4 GHz by Auriemma *et al.* (1977) and Windhorst (1984), and at 2.4 GHz by Franceschini *et al.* (1988) were shifted to 5 GHz assuming a mean spectral index of −0.7 and are shown for comparison, as are the earlier 5-GHz measurements by Ekers & Ekers (1973).

The luminosity functions agree well for strong sources (10^{24}–10^{26} W Hz^{-1}), but the derived space density of weaker sources is about five times higher than that found by Auriemma *et al.* (1977). The excess might be partly due to a population of flat-spectrum sources at 5 GHz, but the good agreement at the faint end with the recent 2.4-GHz determination by Franceschini *et al.* (1988) who used a completely independent sample suggests that Auriemma *et al.* seriously underestimated the local space density of weak radio sources.

4 Radio emission from nearby E and S0 galaxies

4.1 COMPACT AND EXTENDED RADIO EMISSION

Fig. 3 shows the fractional radio luminosity function (FLF) for our combined sample of E and S0 galaxies. The FLF was calculated using a Kaplan–Meier estimator (Feigelson & Nelson 1985; see also Appendix A), for both the total radio power, P_{tot}, and the power in the unresolved central component, P_{core}.

Where extended emission is present, the central component typically contains about 10 per cent of the total flux, independent of M_B, though the ratio P_{core}/P_{tot} shows considerable scatter (see Table 2). Part of this scatter may be observational, since emission on large scales or at low surface brightness would not have been detected in our maps.

Table 5. Corrected flux densities for galaxies observed at Parkes by Sadler (1984c)

Galaxy	PKS corrected flux density 2.7 GHz (mJy)	5.0 GHz (mJy)	Spectral index
NGC1553	< 30	< 30	
NGC1947	18	18	0.0
367-G08	< 30	< 30	
IC2200A	< 30	< 30	
NGC6758	42	28	−0.7
IC4991	29	20	−0.7
286-G50	< 30	< 30	

NGC 1553: The source detected at Parkes is not this galaxy.

NGC 1947: The MOST map reveals a source 4 arcmin south-east of the galaxy and a second source coincident with the nucleus with a flux density of 18.6 mJy at 843 MHz. Both sources are unresolved (<40 arcsec in size). The second source would have confused the Parkes observation at 2.7 GHz, but not at 5.0 GHz, so the corrected flux density of NGC 1947 is 18 mJy at both frequencies and the galaxy has a flat spectrum.

367-G08: There are several confusing sources in the field, the strongest (19 mJy) about 1 arcmin north of the galaxy. The galaxy itself is not detected.

IC 2200A: A check of the galaxy position indicates that the source listed by Sadler (1984c) is associated with the S0-a galaxy IC 2200 rather than IC 2200A. The optical emission lines reported by Bergvall *et al.* (1978) are also associated with IC 2200, not IC 2200A.

NGC 6758: There is a confusing source 1.5 arcmin south-east of the nucleus, with flux density 20 mJy, while the central source has a flux density of 61.2 mJy at 843 MHz. Disney & Wall (1977) measured a peak flux density of 25 mJy at 5 GHz.

IC 4991: The VLA map shows a second source about 5 arcmin from the galaxy. This would have confused the Parkes detection at 2.7 GHz (8-arcmin beam) but not at 5.0 GHz (4-arcmin beam), and would account for the unusually steep spectral index of −1.6 observed at Parkes.

286-G50: The VLA map shows a double source about 1.1 arcmin east of the nucleus of the galaxy. This is responsible for the Parkes detection, but is not associated with the galaxy.

4.2 THE NATURE OF THE UNRESOLVED VLA SOURCES

Most of the new VLA detections are unresolved radio sources associated with the nuclei of early-type galaxies, and their spectral indices are unknown since they were observed at only one frequency. However, it is likely that these weak sources (with radio powers of $10^{19.5}$ to

Table 6. Local radio luminosity function for E and S0 galaxies at 5 GHz.

log $P_{5.0}$ (W/Hz)	N	$\Phi(P)$ (/mag Mpc^3)	Error
25.8	3	2.11×10^{-8}	1.22×10^{-8}
25.0	28	6.57×10^{-7}	1.24×10^{-7}
24.2	17	3.86×10^{-6}	0.94×10^{-6}
23.4	6	1.16×10^{-5}	0.47×10^{-5}
22.6	8	1.29×10^{-4}	0.46×10^{-4}
21.8	10	1.30×10^{-4}	0.41×10^{-4}
21.0	12	2.89×10^{-4}	0.83×10^{-4}
20.2	10	8.26×10^{-4}	2.61×10^{-4}
19.4	3	2.13×10^{-3}	1.23×10^{-3}

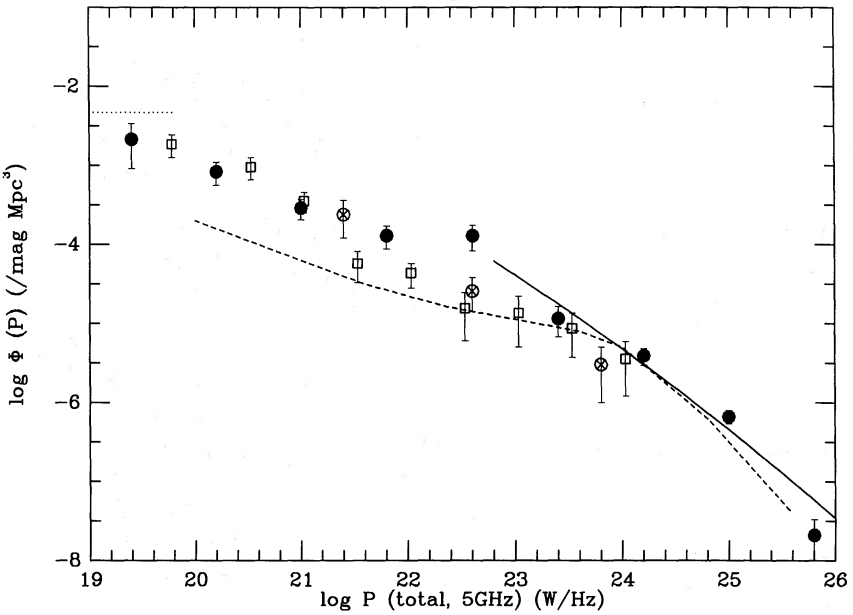

Figure 2. The radio luminosity function at 5 GHz for the combined VLA/PKS/WP sample. Previous determinations by Auriemma *et al.* (1977, dashed line) and Windhorst (1984, solid line) have been shifted to 5 GHz assuming a mean spectral index of -0.7, and are shown for comparison. The three points marked ⊗ are from Ekers & Ekers (1973), while open squares represent the local radio luminosity function derived by Franceschini *et al.* (1988). The dotted horizontal line at the left of the plot marks the space density of all E and S0 galaxies brighter than $M_B = -18.0$, which is $10^{-2.33}$ galaxies mag^{-1} Mpc^{-3} (Sadler 1982).

10^{21} W Hz^{-1}) arise from the same non-thermal emission mechanism which operates in more powerful radio galaxies. This is not only because their radio properties are continuous with those of more powerful objects, but because (as shown below) other plausible sources of radio emission (H II regions, planetary nebulae, supernova remnants) cannot account for the observed radio luminosity in galaxies brighter than $M_B = -18$.

For thermal emission from H II regions and planetary nebulae, the ratio of the (monochromatic, 5 GHz) radio flux (in mJy, where 1 Jy $= 10^{-26}$ W m^{-2} Hz^{-1}) to the Hβ emission-line flux (in W m^{-2}) is

$$S_{5.0}/S_\beta = 3.28 \times 10^{15}$$

(Terzian 1968). Putting $S_\alpha = 3S_\beta$, the expected ratio of 5-GHz radio power (in W Hz^{-1}) to Hα emission-line luminosity (in W) is

$$P_{5.0}/L_\alpha = 9.84 \times 10^{-14}.$$

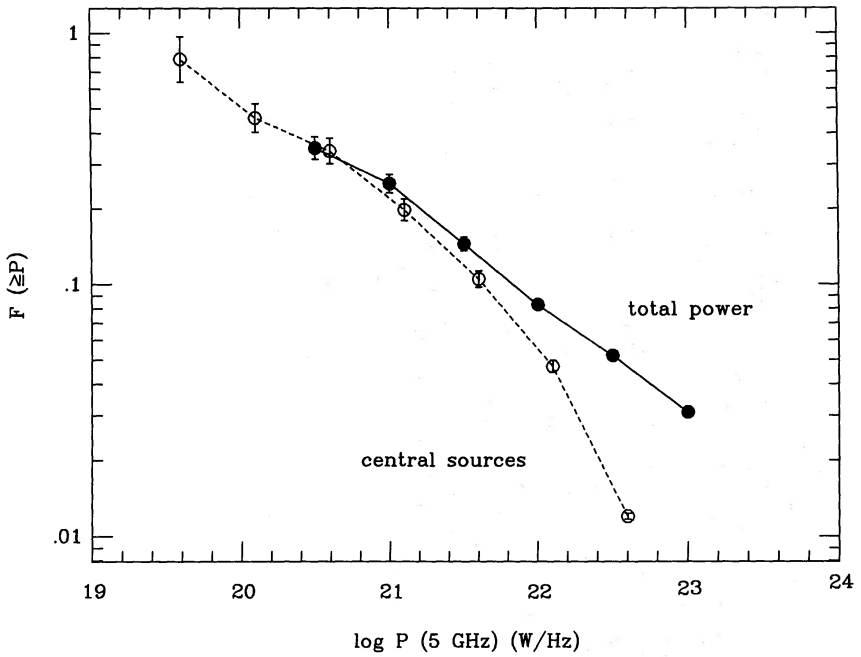

Figure 3. The (integrated) fractional luminosity function (FLF) for elliptical and S0 galaxies (brighter than $M_B - 19.0$) at 5 GHz, derived using the Kaplan–Meier estimator (Feigelson & Nelson 1985). Filled circles represent the total radio power for detected sources, while open circles show emission from unresolved central sources, measured from the VLA maps.

The galaxies in our survey have typical Hα luminosities of 10^{31}–10^{32} W (see Section 6), but the observed [N II]/Hα line ratios imply that most of this gas is ionized by non-stellar means, and is not in H II regions (Phillips *et al.* 1986). Even if the observed optical emission *were* thermal, the maximum contribution would be about 10^{19} W Hz^{-1} at 5 GHz, and thus emission from H II regions cannot account for the observed radio flux.

The contribution of supernova remnants to the radio emission from external galaxies has been discussed by many authors (Rieke *et al.* 1980; Condon *et al.* 1982; Jenkins 1984), though these calculations are based on supernova remnants in our own Galaxy, where the interstellar medium is very different from that in an E/S0 galaxy. A radio output of 10^{20} W Hz^{-1} at 5 GHz would require a supernova rate of 0.02 yr^{-1} in the nucleus. This in turn would require some 10^8 $M_\odot$ of young stars, i.e. a substantial fraction of all stars present in the region of interest, which is no bigger than a kiloparsec. Recent starbursts of this size are ruled out by spectroscopic studies of the stellar population (Rose 1985), and by the observed supernova rate in E and S0 galaxies (Tammann 1977; van den Bergh, McClure & Evans 1987). A realistic upper limit for the contribution of supernova remnants to the 5-GHz emission from the centre of a typical early-type galaxy is 10^{18} W Hz^{-1} (assuming 10^9 $L_\odot$ for the luminosity of the relevant nuclear regions).

With this in mind, we will assume for the remainder of this paper that the dominant radio component in all early-type galaxies brighter than $M_B = 18.0$ is synchrotron emission from an active nucleus (e.g. Rees 1978; Blandford & Rees 1978 and references therein). This assumption is not essential to the discussion which follows, but it gives us a framework within which to interpret the observed radio and optical properties. We also caution that the assumption does not hold for galaxies less luminous than about $M_B = -18.0$, as discussed in the following section.

4.3 RADIO EMISSION FROM LOW-LUMINOSITY GALAXIES

Unlike their brighter counterparts, many low-luminosity elliptical and S0 galaxies ($M_B > -18.0$) have emission-line spectra resembling H II-regions, and appear to contain young stars (Phillips *et al.* 1986). Such galaxies are severely under-represented in the present study, which is based on a magnitude-limited galaxy sample. The only H II-region elliptical in the VLA sample is NGC 2328, which has a radio power of $10^{19.4}$ W Hz^{-1} at 5 GHz. If this radio emission is thermal, the expected Hα luminosity is 2.5×10^{33} W, consistent with the observed value.

Low-luminosity 'starburst' galaxies of this kind are unlikely to contribute significantly to the radio galaxy population above 10^{20} W Hz^{-1}, since NGC 2328 is one of the strongest emission-line systems in the Phillips *et al.* sample. However, because their space density is relatively high, they could easily dominate the population below 10^{19} W Hz^{-1}. Further observations of a larger sample of these objects would be valuable in clarifying the nature of their radio emission.

4.4 RADIO POWER AND OPTICAL LUMINOSITY

In an important paper, Auriemma *et al.* (1977) first showed quantitatively that brighter elliptical galaxies are more likely to be radio sources. They analysed a composite, radio-selected sample of galaxies, most of them powerful radio sources by our standards ($P \geq 10^{22}$ W Hz^{-1}).

The radio luminosity function for their sample changed slope at a power P^* between 10^{24} and 10^{25} W Hz^{-1} (see Fig. 2). Above P^*, the luminosity function ρ could be factorized into separate dependences on monochromatic radio power P and optical (blue) luminosity L_B:

$$\rho(P, L_B) \propto L_B^{1.5 \pm 0.2} P^{-2.3 \pm 0.2} \qquad \text{for } P > P^* \tag{1}$$

(Note that the exponent of P in equation (1) is *one less* than the slope measured from a plot of $\rho(P)$ versus $\log P$ because the data are binned in equal logarithmic intervals rather than intervals of equal size.) Below P^*, the influence of L_B on ρ appeared to weaken with decreasing P.

As remarked earlier, the sample analysed by Auriemma *et al.* has few galaxies with radio powers below 10^{22} W Hz^{-1}. We have used the larger sample of low-power galaxies detected in the Parkes and VLA surveys to re-determine the bivariate luminosity function below P^*, and to examine the reported decline in the influence of L_B at lower radio powers.

We combined our Parkes and VLA samples as described in Section 3.1, using the total radio power P and optical luminosity L_B. The combined sample contains 230 galaxies brighter than $M_B = -17.5$, of which 63 (27 per cent) are radio detections. We divided the sample into bins 1 mag wide in L_B, centred at $M_B = -18.0$, -19.0, -20.0 and -21.0, and used the methods of univariate survival analysis (Appendix A) to calculate a fractional radio luminosity function.

We used Avni's estimator (Avni *et al.* 1980), which gives a differential, rather than an integral, estimate of the luminosity function. The statistical errors in adjacent P bins are then nearly uncorrelated, which makes them easier to analyse. By calculating the fractional luminosity function directly, we also eliminate the need to normalize to an uncertain optical luminosity function, which Auriemma *et al.* were obliged to do.

Fig. 4 shows the results for the three brightest bins in M_B (the detection rate in the $M_B = -18$ mag bin was too low to give an accurate luminosity function). The luminosity functions are plotted together in Fig. 5 for comparison. Two different methods were used to calculate the statistical errors arising from the finite size of the sample: a bootstrap, sampling with replacement from the list of galaxies, and a direct Monte Carlo simulation using approximations to the radio and optical luminosity functions (Sadler 1982), plus the known

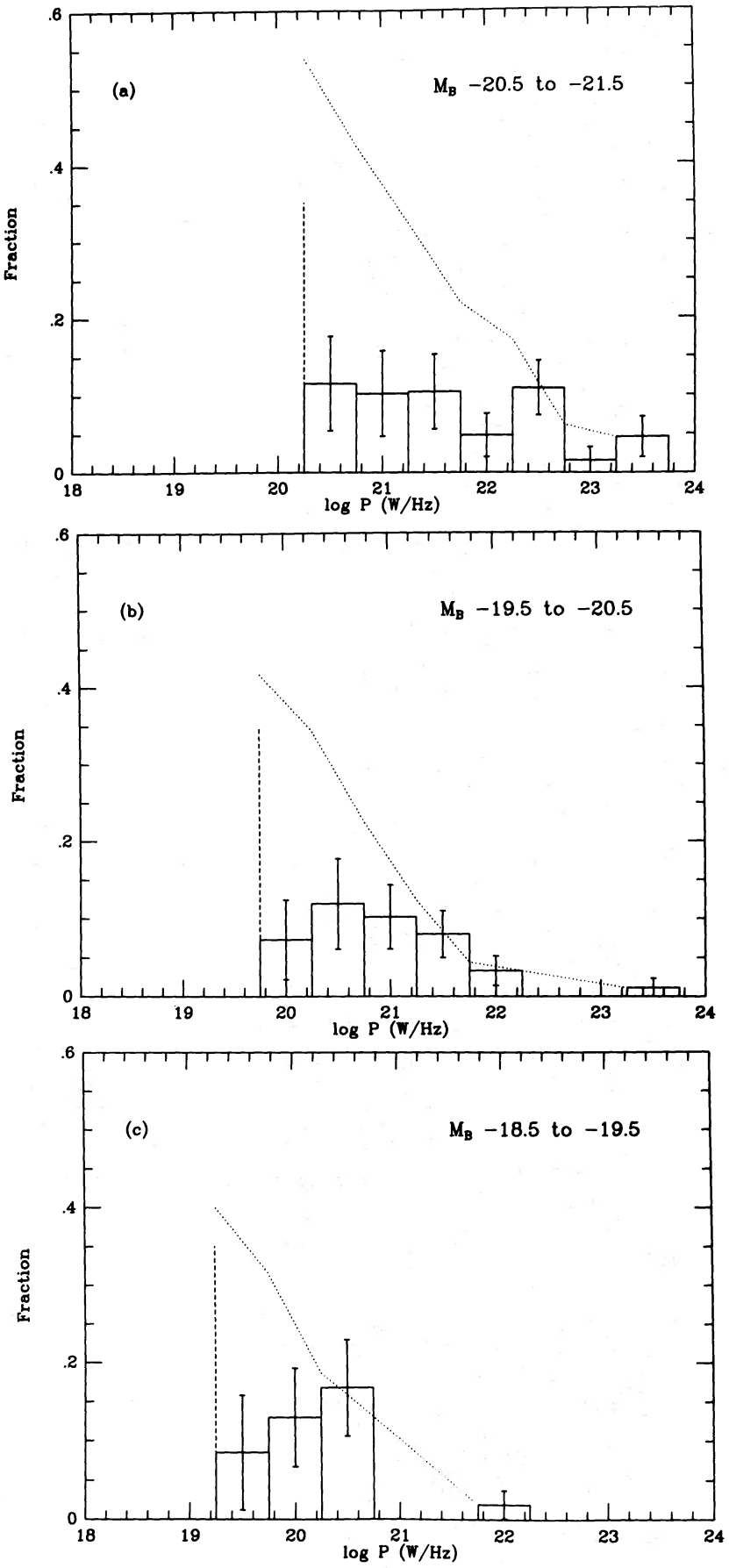

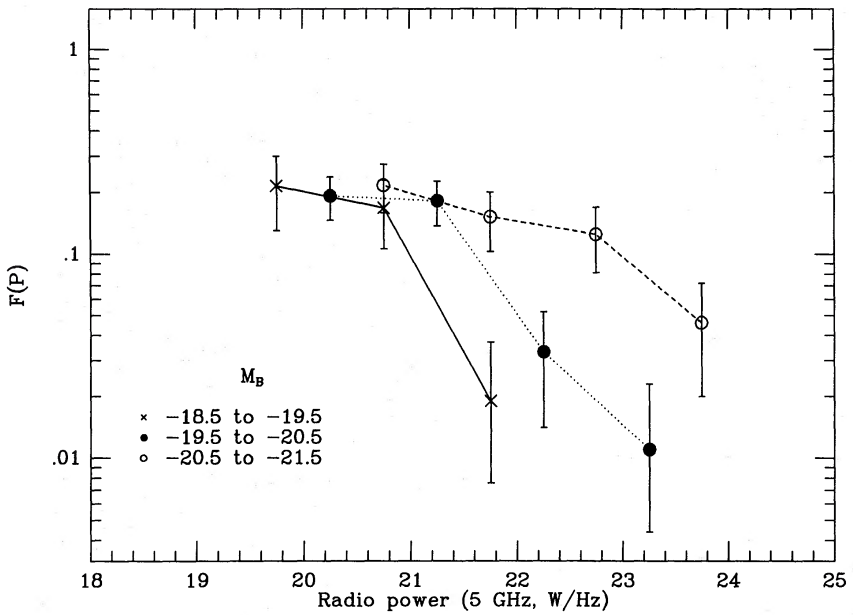

Figure 5. Shows a superposition of the three distributions of $\rho(P)$ in Fig. 4. $\rho(P, L_B)$ has now been calculated in bins 1 dex wide in log P, improving the signal-to-noise ratios in the fainter bins at the expense of resolution. The vertical scale is now logarithmic.

flux limits for these data. Both methods gave similar error estimates. The simulations were also checked for possible systematic errors arising from the wide bins in L_B (see Appendix A), but such errors were found to be negligible.

Is the luminosity function at low radio powers also factorizable into separate dependences on P and L_B, and how are these two quantities related? If we insist on a form for $\rho(P, L_B)$ like that found at higher P, the best fit of an equation like (1) gives

$$\rho(P, L_B) \propto L_B^{0.5} P^{-1.6}.$$

Even if the Auriemma *et al.* form is preserved at low powers, the dependence on absolute magnitude is weaker in the range of P covered by our data.

The data in the range 10^{19}–$10^{20.5}$ W Hz^{-1} are more consistent with $\rho(P, L_B)$ being independent of L_B and inversely proportional to P (so that $F(P)$ appears constant when plotted in equal logarithmic intervals of P, as in Fig. 5).

Above $10^{20.5}$ W Hz^{-1}, there is a transition to the steeper dependence on P found by Auriemma *et al.*, with the change occurring at higher powers for brighter galaxies. This transition appears to be complete by 10^{22} W Hz^{-1}, and the luminosity function then factorizes into the separate dependences on P and L_B found by Auriemma *et al.*

We can rule out a simple horizontal shift of the luminosity function $\rho(P, L_b)$ with increasing L_B. Auriemma *et al.* note that a shift of log P by up to as 0.4 dex mag^{-1} in M_B is not excluded by their data. A shift of this size, with an invariant shape for ρ, brings our luminosity functions for the $M_B = -19$ and $M_B = -20$ bins into agreement, but agreement with the $M_B = -21$ bin

Figure 4. The bivariate luminosity function, $\rho(P, L_B)$ for early-type galaxies in three absolute magnitude bins. The vertical dashed line marks the power below which any remaining galaxies are undetectable in our VLA survey (luminous galaxies are further away on average than less luminous ones, so this limit moves to lower values of P as M_B decreases). The dotted line shows the cumulative fraction of radio-emitting galaxies. Errors were estimated by a bootstrap method described in the text.

would require at least 4–5 times more radio sources of 10^{21}–10^{23} W Hz^{-1} in galaxies fainter than $M_B = -20$ than are actually observed.

Regardless of its detailed form, the distribution $\rho(P, L_B)$ is characterized by a lower typical power for optically fainter galaxies. We used the quantile P_{30}, the power above which 30 per cent of galaxies radiate, as a characteristic radio power. P_{30} is plotted against L_B in Fig. 6, and there is a strong correlation down to powers as low as 10^{20} W Hz^{-1}. A linear fit to $\log P$ and M_B gives

$$P_{30} \propto L_B^{2.2 \pm 0.3}$$

for P in the range 10^{20}–$10^{22.5}$ W Hz^{-1}. (The error bars in Fig. 6 were calculated in the same way as described for the luminosity functions.) Values of P_{30} can also be calculated for the Auriemma *et al.* sample, and are shown in Fig. 6.

The behaviour of P_{30} shows that the *characteristic* radio power of any sample is a strong function of absolute magnitude, even though weak radio sources ($P < 10^{21}$ W Hz^{-1}) are as common in faint galaxies as in brighter ones.

The conclusions of our analysis of the bivariate luminosity function are as follows:

(i) Optical luminosity strongly influences the radio luminosity function down to powers of 10^{21} W Hz^{-1}.

(ii) Above 10^{22} W Hz^{-1}, as Auriemma *et al.* found, brighter galaxies have an increased probability of radio emission across a wide range of powers. The bivariate luminosity function $\rho(P, L_B)$ can be factorized into separate dependences on L_B and P.

(iii) From $10^{20.5}$ to 10^{22} W Hz^{-1} there is a transition region where the bivariate luminosity function is not factorizable.

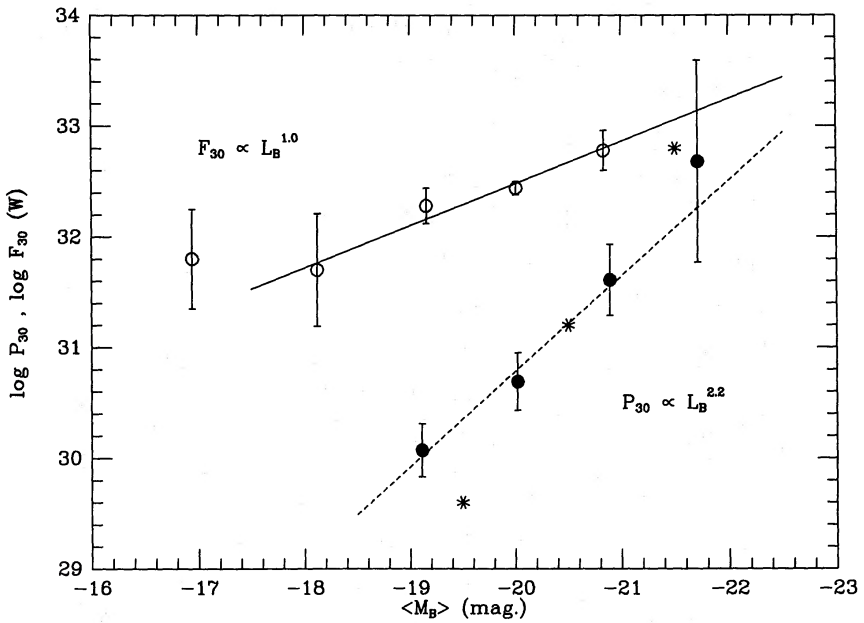

Figure 6. The variation of characteristic radio powers and emission-line luminosities with L_B. Filled circles denote values of P_{30}, the total 5-GHz power exceeded by 30 per cent of galaxies, in several absolute magnitude bins, for the combined PKS/VLA sample. The starred points are values of P_{30} calculated from Auriemma *et al.* (1977). The radio luminosity has been converted to an integrated output in watts assuming a bandwidth of 10^{10} Hz. Open circles are values of F_{30}, the λ6584 [N II] emission-line luminosity exceeded by 30 per cent of the galaxies in each M_B bin. The lines show the slope of linear fits to the P_{30}–L_B and F_{30}–L_B relations.

(iv) Below $10^{20.5}$ W Hz^{-1}, down to the lowest powers we could observe, $\rho(P, L_B)$ is essentially independent of L_B. We have not yet seen the low-power turnover in $\rho(P, L_B)$ which must eventually be imposed by the normalization constraint.

It is remarkable that a global property like L_B, which is determined by the stellar population on scales of tens of kiloparsecs, should be closely associated with so small an object as an active nucleus. It is particularly interesting that we can demonstrate a P–L_B connection for a sample in which most of the radio sources are unresolved, and hence smaller than a kiloparsec in size.

So far, we have treated the whole sample of early-type galaxies together. The large range in P observed at all values of L_B, however, suggests that other factors besides L_B may influence the strength of the radio source in an individual galaxy. In the following section we look at possible differences in the radio properties of elliptical and S0 galaxies, while in Section 6 we explore the relation between radio emission and the central gas content of an early-type galaxy.

5 Comparison of E and S0 galaxies

5.1 COMPARISON OF THE RADIO LUMINOSITY FUNCTIONS

In any galaxy sample selected by apparent magnitude, the elliptical galaxies will be about a magnitude more luminous, on average, than the S0s (e.g. Sadler 1982). At least half the light in a typical S0 galaxy comes from the disc component (Dressler & Sandage 1983), so the difference is even larger if we consider bulge luminosity rather than total luminosity. It is important to keep these differences in mind when comparing the radio properties of elliptical and S0 galaxies.

Fig. 7 shows the integrated fractional luminosity function (FLF) for elliptical and S0 galaxies in several luminosity bins. We used classifications from the ESO/Uppsala Catalogue (Lauberts

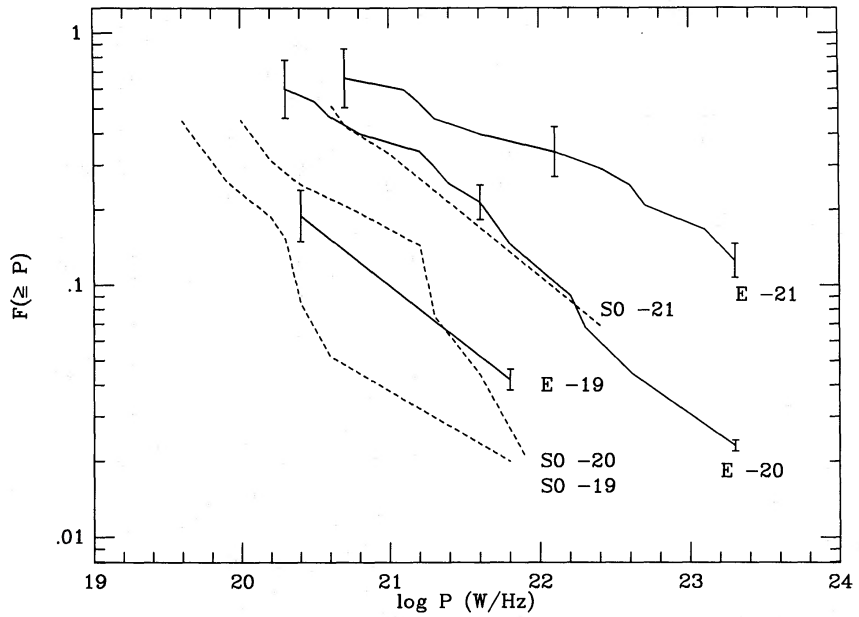

Figure 7. The FLF for ellipticals and S0s separately. This is now a trivariate luminosity function $\rho(P, L_B, \text{type})$. Because of the large number of bins into which the sample must now be split, and the small number of detections in some bins, we show the integrated luminosity function, and the results should be considered as qualitative only.

1982), as listed in Table 4. The FLF for S0s at any given value of M_B is about a factor of 3 lower than that for ellipticals, but the two FLFs can be brought into agreement by assuming that the bulge contributes half the total light of an S0 galaxy. If so, central radio sources are about as common in elliptical galaxies as in S0s with similar-sized bulge components.

It is generally believed that most S0 bulges are oblate and rotationally supported, while bright ellipticals are triaxial and flattened by velocity anisotropies (Davies *et al.* 1983; Binney 1985). The kinematics of gas in the innermost kiloparsecs of a galactic bulge depend sensitively on the shape of the stellar potential (Habe & Ikeuchi 1985). If radio sources are fuelled by gas reaching the nuclear regions from large distances, then the shape of the Galaxy ought to be relevant, and it is surprising that a simple scaling by bulge luminosity brings the radio luminosity functions for the two Hubble types into agreement.

Our results are consistent with those of Hummel & Kotanyi (1982), who compared the integrated FLFs for E and S0 galaxies. They noted that the central sources in S0s were on average a factor of 10 weaker than those in elliptical galaxies, and we find a similar result (for example, 30 per cent of elliptical galaxies in our sample have central sources stronger than $10^{20.9}$ W Hz^{-1}, while the 30 per cent level for the central sources of S0s lies at $10^{20.0}$ W Hz^{-1}).

It has been suggested that radio-emitting S0 galaxies are misclassified ellipticals, and that true S0 galaxies do not sustain radio sources (Hummel & Kotanyi 1982). In the next section, we discuss the apparent shapes of elliptical and S0 galaxies, and show that most radio-emitting S0 galaxies are typical members of their class and unlikely to be misclassified ellipticals or spirals.

5.2 RADIO POWER AND GALAXY SHAPE

Several authors (Heeschen 1970; Hummel *et al.* 1983; Disney *et al.* 1984) note that radio-emitting elliptical galaxies are rounder than average, and attribute this to differences in the rate of gas flow to an active nucleus in round and flat galaxies.

Here, we use survival analysis techniques to re-examine the relation between radio power P and axial ratio for early-type galaxies. We use the BHK method (Brown, Hollander & Korwar 1974; described by Isobe, Feigelson & Nelson 1986) to test for correlations between uncensored variables (axial ratio and M_B) as well as between a censored and an uncensored variable (axial ratio and P). The test is a generalized form of the non-parametric Kendall's rank correlation, adapted for censored data sets, and uses both detections and upper limits.

We discuss elliptical and S0 galaxies separately, since they have different distributions of axial ratio.

5.2.1 S0 galaxies

Axial ratio $\log(a/b)$ correlates with M_B for S0 galaxies in the PKS/VLA sample, with brighter S0s being rounder on average than fainter ones. Sadler (1982) discussed this effect, and showed that it was not an artefact of the 1-arcmin-diameter cut-off in the ESO/Uppsala catalogue from which the galaxies were selected. It may arise from a real difference in the properties of bright S0s compared to fainter ones (for example, a change in bulge-to-disc ratio with luminosity), or from contamination of the S0 sample by brighter ellipticals.

In spite of the M_B–$\log(a/b)$ correlation, there is no significant correlation between axial ratio and P. The radio-emitting S0 galaxies span a large range in $\log(a/b)$, with a median value of 0.21 for galaxies with $P \geq 10^{20.5}$ W Hz^{-1}. The median value of $\log(a/b)$ for S0s with radio powers below $10^{20.5}$ W Hz^{-1} is 0.24, so, in contrast to Ekers & Ekers (1973), we do not find that S0 galaxies with radio sources are as round as a typical elliptical. Our VLA survey reaches

characteristic radio powers 10 times lower than the Ekers & Ekers (1973) sample, and the higher detection rate means our results are less affected by a small number of contaminating sources. It is also likely that our S0 sample is genuinely less contaminated than theirs, since the quality of plate material available for classifying large galaxy samples has improved markedly during the past decade.

Among the S0 galaxies in our sample with $P \geq 10^{20.5}$ W Hz^{-1}, there are rather more (7/16, or 44 per cent) rounder than $\log(a/b) = 0.10$ than might be expected (25 per cent of the 77 well-classified S0 galaxies in the RSA are as round as this), though the excess is significant only at the 20 per cent level in a χ^2 test. Thus we believe that our sample of S0 galaxies is not significantly contaminated by ellipticals, and we find no correlation between radio power and apparent flattening for S0 galaxies.

5.2.2 *Elliptical galaxies*

M_B and $\log(a/b)$ are uncorrelated for elliptical galaxies in the PKS/VLA sample, in agreement with an earlier study by Leir & van den Bergh (1977). This is reassuring because we can study the relation between radio power and axial ratio directly, without needing to account for a mutual correlation with L_B.

As for S0 galaxies, the BHK test shows no correlation between $\log(a/b)$ and P for the elliptical sample, implying that radio luminosity is unrelated to galaxy shape for the relatively weak radio sources studied here. A similar result was found by Dressel (1981) for a large sample of galaxies observed at 2.4 GHz.

Fig. 8 shows the fractional luminosity function $\rho(P)$ for elliptical galaxies in the PKS/VLA sample rounder and flatter than $\log(a/b) = 0.180$ (E3.4), as well as for S0 galaxies with no restriction on $\log(a/b)$. We originally divided the ellipticals into three bins in $\log(a/b)$, 0.000 to 0.079, 0.080 to 0.179 and 0.180 and flatter, with the divisions chosen to give the same number of galaxies in each bin, and also to investigate the possibility that elliptical galaxies with

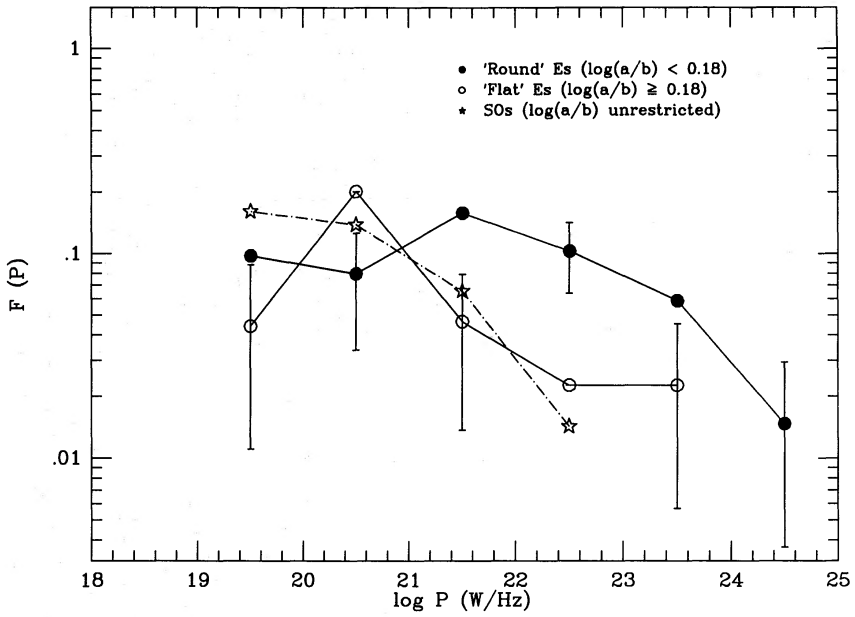

Figure 8. $\rho(P)$ for 'round' and 'flat' elliptical galaxies [with $\log(a/b) < 0.180$ and ≥ 0.180, respectively, where a and b are the major and minor axis diameter], and for S0 galaxies without restriction on shape. The error bars on the S0 points have been omitted for clarity, but are similar to those for the elliptical galaxies.

$\log(a/b) > 0.18$ are deficient in radio sources (Disney *et al.* 1984). The FLF for the flattest ellipticals ($\log(a/b) \geq 0.180$) lies below that for rounder galaxies at radio powers above 10^{21} W Hz^{-1}, though the difference is not statistically significant for the distribution as a whole.

5.3 COMPARISON WITH EARLIER WORK

We re-examine some earlier findings by Hummel *et al.* (1983) and Disney *et al.* (1984) that radio-emitting elliptical galaxies are drawn from a rounder parent population than their 'radio-quiet' counterparts.

To minimize the effects of misclassification, we compiled a new sample of 92 well-classified (from plates taken with a 2.5- or 5-m telescope) elliptical galaxies from the *Revised Shapley–Ames Catalog* (Sandage & Tammann 1982; RSA). Most of these galaxies have been surveyed at 5 GHz by Birkinshaw & Davies (1985), Impey, Wynn-Williams & Becklin (1986), Disney & Wall (1977) or ourselves, and 72 are either detected or have upper limits below 10^{21} W Hz^{-1}. We used the E0–E7 ellipticity classifications from the RSA and binned the sample in $\log P$ as shown in Table 7.

All galaxies with $\log P < 23$ have the same ellipticity distribution, but the six most powerful radio sources lie in galaxies rounder than E1. Whether one sees a relation between radio power and axial ratio in any given radio survey depends strongly on the detection limit of that survey and on the power at which one chooses to divide 'radio' and 'non-radio' galaxies. If we split the RSA sample at $\log P = 21.25$ (the value used by Disney *et al.* (1984), converted to $H_0 = 100$ km s^{-1} Mpc^{-1}) and at $\log P = 21.0$, we have:

$\log P_{5.0}$	>21.25	<21.25	$\log P_{5.0}$	>21.0	<21.0
E0–E3	24	29	E0–E3	25	27
E4–E7	3	18	E4–E7	7	13

As before, we take the cut-off between 'round' and 'flat' ellipticals at E3.4 ($\log(a/b) = 0.18$). For the higher cut-off in $\log P$, the deficiency of 'flat' radio galaxies is significant at the 5 per cent confidence level in a χ^2 test, while for the lower cut-off there is no significant difference between 'round' and 'flat' galaxies. Any apparent difference in the radio properties of round and flat ellipticals probably depends critically on the extent to which the 'radio galaxy' sample is diluted by low-power sources. In the Disney & Wall (1977) sample, 29 per cent of detected galaxies lie above 10^{23} W Hz^{-1}, while in our VLA sample the fraction is only 10 per cent.

In summary, our results do not conflict with previous work if radio sources with $P > 10^{23}$ W Hz^{-1} reside mainly in round elliptical galaxies, while weaker sources occur in galaxies of all shapes.

A more detailed study of the influence of galaxy shape on radio emission is unlikely to be justified until we have better morphological data (for example, bulge/disc deconvolutions

Table 7. Median ellipticity as a function of radio power.

$\log P_{5.0}$ (W Hz^{-1})	N_{gal}	Median ellipticity
> 23	6	E0
22–23	8	E2.5
21–22	18	E2.5
< 21	40	E2
All	72	E2.5

based on accurate surface photometry) for a large sample of galaxies, as well as some way of estimating the true shapes of ellipticals, given that many of them are likely to be triaxial (Binney 1985). Recent work by Bender, Döbereiner & Möllenhof (1987) shows the kind of results which might arise from such a study.

6 Ionized gas and radio emission

6.1 THE GAS CONTENT OF EARLY-TYPE GALAXIES

Several authors (Disney & Cromwell 1971; Ekers & Ekers 1973; O'Connell & Dressel 1978) have discussed the optical spectra of early-type galaxies with central radio sources and pointed out that a large fraction show emission lines of [O II] λ3727 Å. A weaker correlation of radio continuum emission with the presence of H I gas has also been suggested (Hummel *et al.* 1983; Jenkins 1983), though Knapp (1987) found no correlation between H I content and continuum radio power. Kotanyi & Ekers (1979) noted that extended radio sources in dust-lane galaxies tend to align perpendicular to the dust lane, and suggested that the rotation axis of dust and gas in a galaxy is related to the mechanism responsible for radio emission.

Contrary to the classical picture of elliptical galaxies as gas-poor systems, recent observations show that many of them contain substantial amounts of gas. X-ray observations (Biermann & Kronberg 1983; Nulsen, Stewart & Fabian 1984; Forman, Jones & Tucker 1985) reveal that bright elliptical galaxies are surrounded by hot (10^7 K) gaseous coronae with masses of 10^9 to 10^{10} $M_\odot$, and the dust content of E and S0 galaxies (Sadler & Gerhard 1985; Jura 1986) suggests that the inner few kiloparsecs contain 10^6–10^7 $M_\odot$ of neutral hydrogen (assuming a gas-to-dust ratio similar to that in our own Galaxy).

Caldwell (1984) and Phillips *et al.* (1986) have shown that weak optical emission lines occur in the central regions of many E and S0 galaxies, and that the central kiloparsec typically contains 10^3 to 10^5 $M_\odot$ of ionized gas. Such an amount of gas, if it could be transferred steadily to the nucleus, is enough to sustain a radio source of modest power (Gunn 1979), and from their gas content alone it seems plausible that most bright ellipticals and S0s could sustain such a radio source. The emission-line spectra, and thus presumably the gas content and physical conditions, in the central regions of ellipticals, S0s and (early-type) spiral bulges are all similar.

6.2 STELLAR LUMINOSITY AND OPTICAL EMISSION LINES

Before examining the relation between radio properties and emission from ionized gas at 10^4 K, we discuss the important result of Phillips *et al.* (1986) on the relation between optical emission lines and absolute magnitude. Their sample included most of the galaxies in the combined Parkes and VLA surveys. Spectra of the nuclei of more than 200 galaxies were taken in the Hα/[N II] region, with detection limits usually 0.5–1.0 Å in equivalent width. Emission lines of [N II] λ6584 Å or Hα (but mostly the former) were detected in 55 per cent of the galaxies. Phillips *et al.* found no strong correlation of the emission lines with other properties, with one important exception: the emission-line luminosity F of the nitrogen line rose roughly linearly with the integrated blue luminosity L_B, though with considerable scatter. This result was established by a fairly elaborate analysis of the bivariate luminosity function in F and L_B. Much effort was devoted to the derivation of this function by the maximum volume method, for which the selection effects in the data have to be well understood.

We have re-derived the relation between F and L_B by the more direct methods of survival analysis. The procedure was similar to that described in Section 4.4 and readers are referred to Appendix A for technical details. As before, a detailed error analysis was an important feature of the new derivation.

Fig. 9 shows the differential fractional luminosity function, $\phi(F, L_B)$ as a function of F in 1-mag bins of L_B. The results are similar to those derived by Phillips *et al.*; in particular, the characteristic emission-line luminosity increases for brighter galaxies. This can be summarized by using the 30 per cent point of ϕ, F_{30}.

Fig. 6 shows F_{30} as a function of M_B. A relation

$$F_{30} \propto L_B^{\beta}$$

fits the data well, with $\beta = 1.0 \pm 0.3$ if we leave out the $M_B = -17$ mag data point. As remarked earlier (Section 4.3), galaxies as faint as -17 mag may have rather different emission-line properties from more luminous ellipticals. It has thus been established by two different techniques (V/V_{max} and survival analysis) that characteristic emission-line luminosities like F_{30} are closely proportional to L_B. The error analysis, again using two methods (bootstrap and Monte Carlo), gives confidence that the statistical errors are accurately assessed and the result is real. Finally, as before, the methods were able to recover input parameters (β is the one of interest here) reliably in direct simulations.

Fig. 6 also shows how the total energy emitted at radio wavelengths and in optical emission lines varies with M_B. We assume a flat spectral index for the radio sources and a high-frequency cut-off at 10 GHz, so the 'total' radio luminosity is taken as 10^{10} times the monochromatic luminosity at 5 GHz. The optical emission-line luminosity is for the [N II] line only, and so is a lower limit. Nevertheless, the [N II] emission-line luminosity exceeds the total radio luminosity until we reach bright galaxies with M_B around -22 mag. This is also the point at which radio structures commonly begin to be spatially extended outside the nuclear region.

6.3 OPTICAL EMISSION LINES AND THE CENTRAL RADIO SOURCE

Is radio emission directly linked to the presence of optical emission lines like [N II] λ6584? The results of Sections 4.4 and 6.2 show that testing for such a correlation is not straightforward. There are four variables for each galaxy: L_B, P, F and distance. There are intrinsic F–L_B and P–L_B relations, as well as false correlations between distance and the luminosities of detected objects which can cause bogus mutual correlations. Making use of upper limits can circumvent the latter problem.

Fig. 10 shows scatter plots for the P–M_B, F–M_B and also P–F relations. Both detections and upper limits are plotted. We do not know what kind of relation between F and P to expect. It should *not* be based on quantities like the equivalent width, which is determined largely by observational factors and by the distance of the galaxy. An attempt to overcome the distance dependence by working with flux densities, rather than intrinsic quantities, is not obviously useful (Isobe *et al.* 1986). Connections between variables like P and L_B show so much scatter that notions of linear correlation between quantities are of doubtful use, and efficient methods of analysis must be employed to find *any* relationships. Combining our radio data with the optical observations by Phillips *et al.*, we have 208 useful galaxies of which only about 15 per cent are detected in both radio and [N II]. Nearly half the data are doubly censored, so we must try to use these upper limits.

Schmitt (1985) has proposed an elegant and powerful solution. It is straightforward to produce a two-dimensional analogue of the Avni estimator (Appendix A), using maximum likelihood. The rather more difficult problem of solving the resulting equations, and ascribing significance to the results, is discussed in Appendix B. What results is a maximum-likelihood

Figure 9. The distribution of F, the luminosity in the [N II] emission line, as a function of absolute magnitude (analogous to Fig. 4).

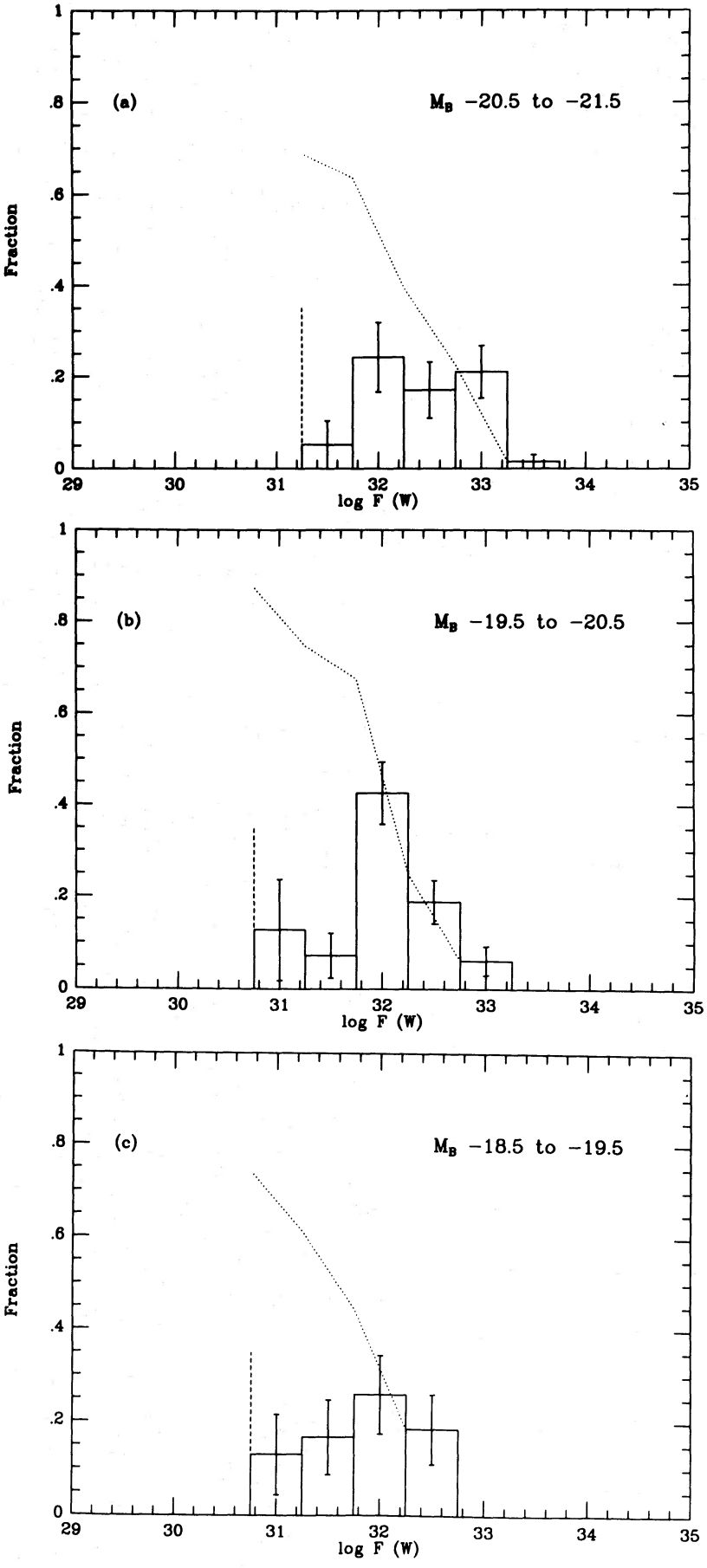

estimate of the bivariate luminosity function $\xi(F, P)$, where the censoring of both variables is accommodated. If one also calculates the univariate functions $\rho(P)$ and $\phi(F)$, then a likelihood ratio will test the null hypothesis that

$$\xi(F, P) = \rho(P)\,\phi(F).$$

This is exactly the test we need, since it is sensitive to *any* relationship which may exist between F and P. It tests whether or not these two variables are statistically independent, the most general question which can be asked about any possible connection between them. The decisive statistic

$$\Delta = -2\log\left(\frac{\text{likelihood of factorizable solution}}{\text{likelihood of fully bivariate solution}}\right)$$

is distributed approximately as χ^2 (Appendix B). To apply the test, we needed to bin the data into a matrix of F–P cells in F and P. These were chosen to be 0.5 by 1.0 dex in size. To populate the matrix adequately, we also had to bin in L_B, which in principle poses difficulties because of the mutual correlations involved (see Appendix B). We chose to add together the $M_B = -19$, -20 and -21 mag bins used earlier (Section 4.4), and later in this section we discuss the errors this introduces.

6.4 RESULTS OF THE BIVARIATE F–P ANALYSIS

The first four arrays in Table 8 give the binned detections and the singly censored and doubly censored observations, while the final array gives the calculated bivariate luminosity function. The data are also plotted in Fig. 10. Table 8 includes galaxies where radio flux densities or limits were known, but no emission-line measurements were available from the Phillips *et al.* (1986) survey. For these galaxies, we set $F < 10^{33.5}$ W, a plausible upper limit. Such galaxies do not contribute to the determination of the bivariate luminosity function, but help in improving the signal-to-noise ratio of the univariate luminosity function which is used as part of the likelihood ratio test.

There is no strong correlation between F and P – not even the false one mediated by L_B, which is probably diluted by the wide range of F and P at any fixed L_B. The bivariate distribution function ξ was found by solving the two-dimensional maximum likelihood equations as described in Appendix B; the resulting values are the fifth array. From this, we can calculate the test statistic Δ. Taking into account the uncertainties associated with the various ways of ensuring the normalization of ξ (Appendix B), we find Δ in the range 23 to 34. This is consistent with the null hypothesis, as we expect Δ to be distributed approximately as χ^2 with 40 degrees of freedom.

To assess the significance of Δ more precisely, we calculated its distribution by Monte Carlo methods; it is only asymptotically χ^2, and in any case we need to take account explicitly of the mutual correlations of the variables with L_B alluded to earlier. To calculate the distribution of Δ, we used the same detailed model employed in the error analysis of Sections 4.4 and 6.2. This gives a distribution of Δ subject to a Monte Carlo model which builds-in the separate dependences of $\rho(P)$ and $\phi(F)$ on L_B.

Galaxies were drawn from a distribution of absolute magnitude appropriate to the magnitude limit of the sample, and values of F and P were assigned using analytical forms of $\rho(P, L_B)$ and $\phi(F, L_B)$ fitted to the results of Sections 4.4 and 6.2. Appropriate limits, in flux and equivalent width (Sadler 1982; Phillips *et al.* 1986), were applied to obtain detection rates matching those of Table 4, and the simulated sample, containing 200 model galaxies, was

Table 8. Data in the range $M_B = -18.5$ to -21.5 mag, binned into cells of 1 dex in radio power (in $W\,Hz^{-1}$) and 0.5 dex in emission-line luminosity (in W). (a) Array of detections; (b) array of radio upper limits; (c) array of emission-line upper limits; (d) array of dual upper limits; (e) bivariate fractional luminosity functions.

(a) Array of detections

	18.0	19.0	20.0	21.0	22.0	23.0
29.5	0	0	0	0	0	0
30.0	0	0	0	0	0	0
30.5	0	0	0	0	0	0
31.0	0	0	1	0	0	0
31.5	0	0	1	0	0	0
32.0	0	0	3	2	5	1
32.5	0	0	3	2	0	4
33.0	0	0	0	3	3	0
33.5	0	0	0	0	0	0

(b) Array of radio upper limits

	18.0	19.0	20.0	21.0	22.0	23.0
29.5	0	0	0	0	0	0
30.0	0	0	0	0	0	0
30.5	0	0	0	0	0	0
31.0	0	0	2	0	0	0
31.5	0	2	2	1	0	0
32.0	0	8	6	7	0	0
32.5	0	3	7	5	0	0
33.0	0	0	3	4	1	0
33.5	0	0	0	1	0	0

(c) Array of emission-line upper limits

	18.0	19.0	20.0	21.0	22.0	23.0
29.5	0	0	0	0	0	0
30.0	0	0	0	0	0	0
30.5	0	0	1	0	0	0
31.0	0	0	0	0	0	0
31.5	0	0	2	0	2	0
32.0	0	0	1	2	2	0
32.5	0	0	1	1	0	0
33.0	0	1	0	0	0	0
33.5	0	0	5	9	2	3

(d) Array of dual upper limits

	18.0	19.0	20.0	21.0	22.0	23.0
29.5	0	0	1	0	0	0
30.0	0	0	1	0	0	0
30.5	0	1	3	0	0	0
31.0	0	1	5	4	0	0
31.5	0	6	1	3	0	0
32.0	0	4	5	9	0	0
32.5	0	1	2	3	0	0
33.0	0	0	1	0	0	0
33.5	5	16	11	12	1	0

(e) Bivariate fractional luminosity function

	18.0	19.0	20.0	21.0	22.0	23.0
29.5	0.00	0.00	0.12	0.00	0.02	0.00
30.0	0.00	0.00	0.00	0.00	0.00	0.00
30.5	0.00	0.00	0.00	0.00	0.00	0.00
31.0	0.00	0.00	0.06	0.00	0.00	0.00
31.5	0.14	0.00	0.01	0.00	0.00	0.00
32.0	0.20	0.00	0.04	0.06	0.04	0.01
32.5	0.08	0.00	0.05	0.03	0.00	0.03
33.0	0.04	0.00	0.00	0.05	0.02	0.00
33.5	0.01	0.00	0.00	0.00	0.00	0.00

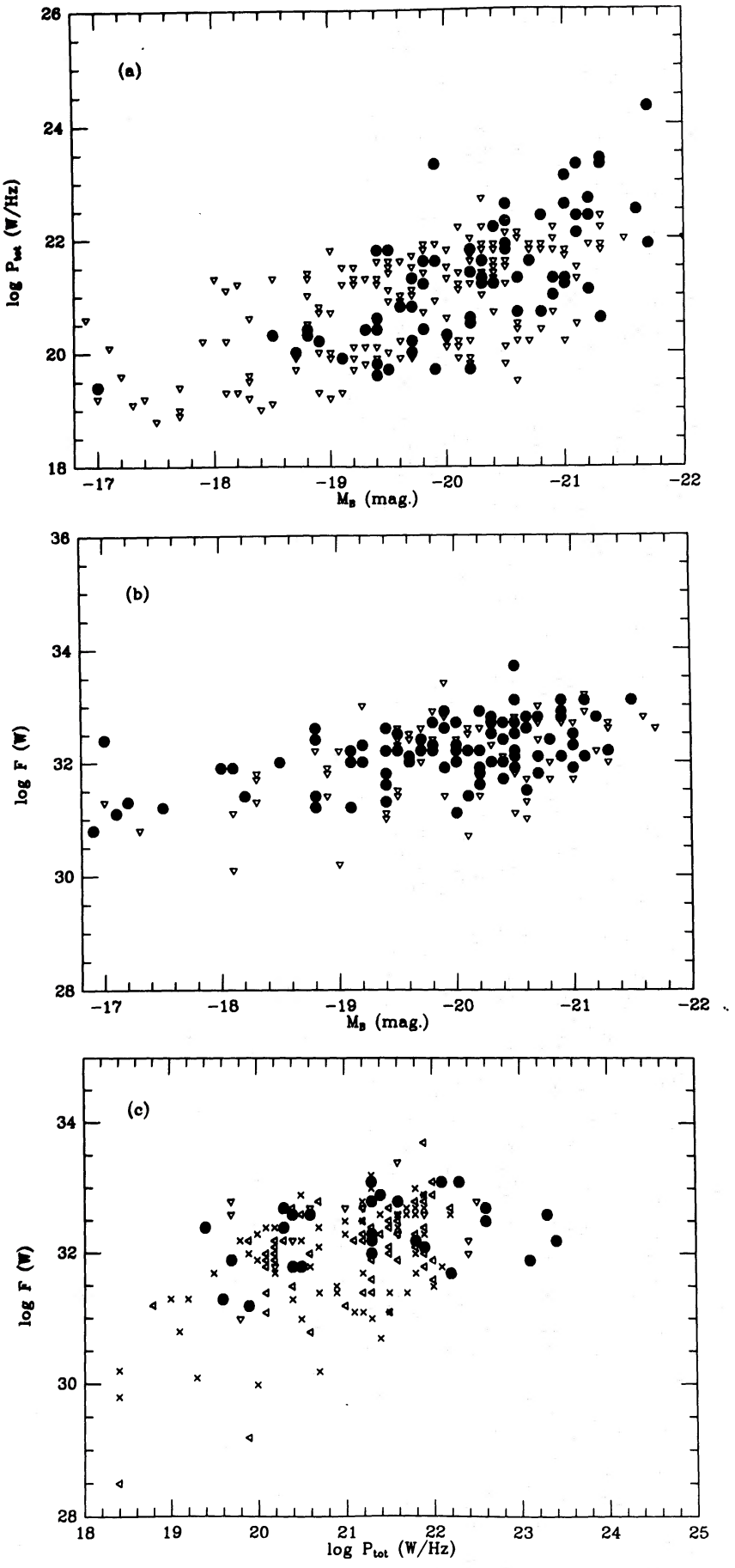

analysed in exactly the same way as the real data. This model assumed there was no relation between F and P, other than that mediated by L_B. After 400 repetitions of this process, an adequate distribution of Δ was obtained. This distribution has a median value of 38, and 10th and 90th percentiles at 30 and 50. We conclude that there is no evidence against the null hypothesis that $\xi(F, P)$ is factorizable into independent distributions of F and P. That is, there is no reason to reject the hypothesis that the total radio power at 5 GHz is unrelated to the [N II] λ6584 luminosity.

How strong a relation between F and P could we have detected, given the size of our sample and the sensitivity of the observations? The problem with testing against a non-null hypothesis is that there are many possibilities. By way of illustration, we examined a model where the emission-line luminosity of each galaxy had added to it an amount proportional to the radio power, i.e.

$$F(\text{total}) = F(\text{initial}) + \kappa P.$$

We chose a value of κ which gave a median enhancement of 16 per cent in F(initial). After adjusting the detection limits to maintain the same detection rates as were observed, we found a marked change in the distribution of Δ. The median was now 46, and the 10th and 90th percentiles 33 and 60. Hence, under this model for κ, the values of Δ would exceed the 10th percentile of the null-hypothesis distribution about half the time. Models with larger values of κ, corresponding to even greater enhancements in the emission-line luminosity, were tried, but it was impossible to match the observed detection rates. This may be taken as a direct demonstration that the effect of P on F is weak.

The conclusion is that our method of analysis should be immune to selection effects, and is sensitive to weak correlations between F and P. None the less we find no evidence that F and P are anything other than statistically independent variables in the range considered ($22 > \log P > 19$, $33 > \log F > 31$, and $-19 > M_B > -21$).

The most powerful radio galaxies have stronger emission lines than other giant elliptical galaxies (e.g. Baum 1987). Thus we may have failed to detect any F–P relation because of the limited range of P in our sample. The preliminary data of Caganoff *et al.* (1988) show a correlation between F and P for powerful (Fanaroff–Riley class II) radio galaxies. This correlation appears to 'switch on' above about 10^{24}–10^{25} W Hz^{-1}, which is also the transition region between class I and class II sources. It is interesting that the correlation found by Caganoff *et al.* becomes obvious only when the total radio output exceeds the luminosity in the emission lines. Most galaxies in our sample have $P \times 10\,\text{GHz} < F$, and the effect of the radio emission may be lost in the 'noise' of emission-line strengths determined by processes unrelated to the radio source itself.

6.5 PREVIOUS WORK: RADIO POWER AND OPTICAL EMISSION LINES

The belief that radio and optical emission are associated even in nearby, relatively feeble galaxies arises mainly from a study by O'Connell & Dressel (1978; OCD), who found that E and S0 galaxies detected at 2.38 GHz usually showed [O II] λ3727 emission lines as well. Furthermore, galaxies with compact radio sources had emission lines more often than those with extended sources.

It is difficult to compare these results, which refer to *apparent* quantities, with ours, which pertain to intrinsic quantities (luminosities). Trends in apparent quantities can be strongly

Figure 10. (a) Absolute magnitude M_B versus total radio power, P; (b) M_B versus [N II] emission-line luminosity F; (c) P versus F, with no restriction on M_B. Filled circles show detections and triangles upper limits while the crosses in (c) are double limits.

influenced by selection effects. In what follows, we compare our sample with OCD in a fairly simple way, then examine the conflicts and possible resolutions in some detail. We are obliged to make the comparison in terms of equivalent width and radio detection, though we stress that conclusions couched in terms of such variables may be unreliable. We are examining the earlier data for consistency with ours in the only way we can, given the limited amount of data available to previous workers.

First consider the apparent correlation between detected [O II] lines and detected radio emission. OCD had data for 57 galaxies. Twenty were undetected at 2.38 GHz and only four of these showed [O II]. Of the remaining 36 'radio galaxies', 21 showed [O II] and 15 did not. (We could not account for one galaxy on the basis of the information given by OCD.) The χ^2 for the 2×2 contingency table summarizing these data is 6.2, formally very significant. In contrast, analysing our magnitude-restricted subsample (Table 4) in the same way gave an insignificantly small χ^2. Thus our sample does not show the effect found by OCD. This is not merely the result of observing a different emission line, since Phillips *et al.* (1986) showed that the equivalent widths of [O II] and [N II] are broadly similar.

What is striking about the OCD sample is the *low* detection rate of [O II], given the way the sample was constructed. Galaxies detected at 2.38 GHz are deliberately over-represented (by about a factor of 10) compared to the original Arecibo survey (Dressel & Condon 1978). Nevertheless, the detection rate achieved by OCD at [O II] is similar to that found by Caldwell (1984), who surveyed 'normal' elliptical galaxies at [O II] with identical sensitivity. The obvious conclusion is that the OCD 'radio galaxies' are unremarkable in their emission-line properties, and that the large value of χ^2 results from the 20 'non-radio' galaxies in the OCD sample being very unrepresentative. Caldwell's data show that OCD should have detected at least twice as many 'non-radio' galaxies at [O II]. Redoing the test with the number of detected 'non-radio' galaxies increased from four to eight reduces χ^2 to 1.1. Thus the OCD result is not robust against small biases in the sample, and the evidence from Caldwell's study is that such biases do exist.

We also examined the possibility that the OCD result was a selection effect, a consequence of the correlation between F and P mediated by a (genuine) mutual relationship with L_B, and a (bogus) mutual correlation with distance. We set up Monte Carlo simulations of the kind described in Section 6.4, and calculated χ^2 for 2×2 tables, classifying galaxies as 'detected' or 'undetected' on the basis of their radio flux density and emission-line equivalent width. There is no intrinsic relation between F and P in these simulations, but we were looking for a bogus correlation between radio and emission-line detectability. Various selection effects were examined. The radio data were assumed to be flux-limited, but several models were used for the equivalent width, depending on whether the aperture used was long and thin (Phillips *et al.*) or large and round (OCD). We also looked at the effect of extended emission-line regions. In practice, the various selection effects cancelled out, and χ^2 was distributed as expected for the case of no correlation.

Our disagreement with OCD is not a selection effect and its resolution must be sought in the nature of the samples used. We stress that the apparent absence of bogus values of χ^2 in these simulations is not a mandate to pursue simple 2×2 tests in search of correlations: in this particular case we could rule out serious selection effects only because we had available a model of the true luminosity functions and selection effects involved. We also found that dividing by radio power, rather than flux density, gave misleading values of χ^2 in the simulated 2×2 tables.

We conclude that there is no tendency for galaxies detected as radio sources to be preferentially detected in emission lines. The earlier result of OCD, indicating that this was so, appears to be the result of an unlucky choice of control sample.

6.6 PREVIOUS WORK: COMPACTNESS AND EMISSION LINES

Previous workers [Ekers & Ekers 1973 (EE); Disney & Cromwell 1971; O'Connell & Dressel 1978 (OCD)] have remarked on a tendency for galaxies with strong nuclear radio emission to be preferentially detected at [O II] λ3727, as well as other emission lines. The available data on the compactness of these radio sources are rather imprecise, and often depend on limited measurements of the visibility function by interferometry. Similarly, the detection (or otherwise) of emission lines is affected by such factors as the size of the aperture used.

We class a galaxy as 'C', or compact, if more than half the radio flux in our VLA maps originates in an unresolved central component. Extended sources are classed as 'X'. Undetected galaxies are automatically excluded from this analysis, so selection effects are introduced from the outset. Combining the radio data with equivalent widths of [N II] measured by Phillips *et al.* (1986) gives the following contingency table:

	C	X
Emission	17	8
No emission	8	5

There is no significant difference, and χ^2 is close to zero. We also derived distribution functions for the C and X classes separately, taking account of upper limits. The distributions are indistinguishable and both classes have median equivalent widths close to 2 Å. This result differs markedly from that of OCD, which in turn is more significant than that of EE. Disney & Cromwell's sample is very similar in content to EE and we will not discuss it here. Since there is inconsistency even among established work on the subject, we comment on EE and OCD in some detail.

EE surveyed a subset of the early-type galaxies in the redshift catalogue of Humason, Mayall & Sandage (1956). The radio structure was classified using four bins ranging from C to X, with the distinction based partly on simple interferometry over a baseline of 17 000 wavelengths, and partly on some fuller syntheses. Detection of [O II] λ3727 by Humason *et al.* was used as the indicator of emission lines. The basic data are as follows:

	C	CX	XC	X
Emission	4	1	3	0
No emission	2	1	1	7

There is only one way to collapse this table into a 2×2 contingency table and still have a statistically significant result: this entails combining C, CX and XC into a single 'compact' category.

OCD drew their sample partly from the flux-limited Arecibo survey (Dressel & Condon 1978) of the Uppsala catalogue. It is clear from their description that the sample is statistically inhomogeneous, as galaxies from other lists were added to increase the number of compact sources. Their definition of compactness depended exclusively on interferometry across a single baseline of 35 000 wavelengths. Observations made by OCD at [O II] λ3727 provided the basis for classifying the emission-line properties of the sample. The resulting 2×2 table is as follows:

	C	X
Emission	16	4
No emission	2	12.

The OCD and EE samples probably have some overlap, since both concentrate on northern early-type galaxies at similar magnitudes.

In Table 9, some properties of each sample are listed to show the difficulty of comparing them. The detection rates have been adjusted to refer to a normal mix of E and S0 galaxies and, in the case of OCD's emission-line data, to the fraction of radio detections given by Dressel & Condon. The significance levels, from Fisher or corrected χ^2 tests (Siegel 1956), are the probability of the observed result arising by chance. The median powers refer only to detected galaxies, as it is only for these that the C–X distinction can be made. OCD do not list redshifts, but their radio detection rate suggests that a flux-limited sample should be biased to even higher powers than EE.

Table 9 shows that the significance level is widely variable and apparently depends on the effective detection rate. As observations become more sensitive, the result weakens. The association between compactness and the presence of emission lines, if real, must therefore be confined to galaxies with strong radio sources, strong emission lines, or both. In our sample, there is no distinct population of strong emission-line galaxies amongst the C class. For galaxies with $\log P > 21.0$, there is still no sign that the compact sources preferentially show emission lines. Any real association would have to be manifest only at $\log P > 22$, where our sample has too few galaxies for useful analysis.

The EE and OCD samples, which can examine this range of powers, are inconsistent in their detection rates and significance levels. The EE sample is more homogeneous, and may be a better guide to the true significance of the association. Even in this case, however, the point at which one chooses to make the arbitrary distinction between 'compact' and 'extended' sources can cause wide variations in the significance level.

We conclude that there is no clear and consistent evidence that optical emission lines occur more often in galaxies which have compact radio sources.

7 Discussion

We now summarize the main results of this work and discuss some simple ideas which may be relevant to their interpretation. Our main conclusions are as follows:

(i) Low-luminosity (10^{19}–10^{21} W Hz^{-1}) radio sources are common in E and S0 galaxies. Even at powers as low as 10^{19} W Hz^{-1}, the radio emission from galaxies brighter than $M_B = -18$ mag is probably non-thermal in origin. In galaxies fainter than $M_B = -18$ mag, thermal emission from H II regions may be the dominant source of radio emission.

(ii) The fraction of early-type galaxies which are strong radio sources (above 10^{22} W Hz^{-1}) increases with optical luminosity. At lower radio powers the optical luminosity has less influence, though a *characteristic* radio power such as P_{30} remains a strong function of absolute magnitude.

Table 9. Comparison of detection rates in three radio surveys.

	OCD	EE	This paper
Flux limit (mJy)	~ 35	200	0.8
Frequency (GHz)	2.38	5.0	5.0
Radio detection rate	0.07	0.10	0.42
Equivalent width limit (Å)	0.6	~ 3	0.5
Emission detection rate	0.22	0.34	0.55
Median log power	> 22.5	~ 22.5	~ 21
Sample size	34	19	38
Significance	< 0.001	0.025	~ 1

(iii) Elliptical galaxies are more likely than S0s to be radio sources at all radio powers above 10^{21} W Hz^{-1}, but this can be explained by the lower luminosity of S0 galaxies (and particularly S0 bulges) relative to ellipticals. For the range of radio powers covered by our sample, elliptical galaxies are detected about as often as S0 galaxies with similar-sized bulges. We see no evidence for any intrinsic difference in the radio properties of elliptical and S0 galaxies once luminosity effects are accounted for.

(iv) We find no correlation between radio power and galaxy shape for low-luminosity radio sources, although there is some evidence that *strong* radio sources ($P \geq 10^{23}$ W Hz^{-1}) occur mainly in round elliptical galaxies.

(iv) Hα/[N II] emission-line luminosity and (monochromatic) radio power are *not* related for galaxies in our sample. Studies of more powerful radio galaxies suggest that a correlation between radio power and emission-line luminosity begins to be seen only when the total radio power exceeds the power in the emission lines, i.e. at radio powers greater than 10^{24} W Hz^{-1}.

(vi) The low-luminosity radio galaxies in our sample emit more energy in the Hα/[N II] emission lines than at 5 GHz, whereas strong radio galaxies typically emit at least twice as much energy in the radio as in emission lines (Baum 1987; Caganoff *et al.* 1988). The characteristic radio and emission-line luminosities for E/S0 galaxies in our sample rise with optical luminosity L_B roughly as

$$P_{30} \propto L_B^{2.2} \quad \text{and} \quad F_{30} \propto L_B.$$

The optical emission lines in 'normal' E and S0 galaxies are significantly stronger (by a factor of at least 10–20 in luminosity) than we would expect just by extrapolating the P–F relation for strong radio galaxies. It is likely that these galaxies contain an extra source of ionizing photons which is not directly related to the radio source.

Some coherence can be given to these observations within the framework of a simple set of ideas, which we discuss here in a qualitative way.

Almost all bright elliptical and S0 galaxies have a central non-thermal radio source. The ability to produce such a radio source is common to all galaxies of this kind, and is not confined to any special class of object. We have also seen that most early-type galaxies have enough gas to fuel a radio source.

The question is why strong radio sources do not occur in *all* early-type galaxies, and why there is such a vast range in radio power among galaxies which appear optically similar.

Below, we list two possible answers. They are not the only possibilities, nor are they mutually exclusive. We discuss the second in more detail, because its consequences may be more directly observable.

(i) The output of the central engine driving the radio source varies with time or depends on small-scale (and hence unobservable) processes which take place within the central few parsecs of the galaxy. The increase of characteristic radio power with optical luminosity could be explained if, for example, larger galaxies had a higher accretion rate of nuclear gas. Galaxies with weaker radio sources might be those where the internal kinematics of the galaxy prevent most of the gas in the central kiloparsec from reaching the nucleus (e.g. Habe & Ikeuchi 1985).

(ii) All galaxies have central engines, but the size and strength of the observed radio source depends on physical conditions within the interstellar medium of each galaxy. An important property of a radio source is the power in the beam emanating from the nucleus. The hot, tenuous gas which pervades early-type galaxies is densest in the centre, and a beam must force its way out against the ram pressure of the hot interstellar medium. It is also vulnerable to flow instabilities, which are most marked for slow, light (i.e. low-power) beams.

Below a certain beam power $B_{\rm crit}$, the beam will be trapped or disrupted near the galactic nucleus, producing a radio source. Above $B_{\rm crit}$, the beam will escape the densest part of the interstellar medium and can propagate freely to large distances. $B_{\rm crit}$ increases with central gas density, which in turn increases with the mass and optical luminosity of the galaxy. Even if the distribution of beam powers is independent of galaxy luminosity (a simple 'null hypothesis'), massive galaxies will trap more of the beams and turn them into radio sources.

In this picture, massive galaxies would be more likely to contain radio sources. There would be a wide range of powers at all sizes of galaxy, given the extra unrelated parameters involved in converting a beam power to a source output. Moreover, even an escaping beam would presumably leave some traces of its passage out of the nucleus. The fact that we are detecting nearly all bright ellipticals above $10^{19.5}$ W Hz^{-1} suggests that such traces involve radiation at or above this level of power.

There are several reasons why an explanation of the P–L_B relation in terms of the interstellar medium is attractive. Fabbiano *et al.* (1987) studied the radio and X-ray properties of a sample of 20 elliptical and S0 galaxies, and found that radio power correlated more closely with X-ray luminosity than with optical luminosity. They showed that the hot X-ray-emitting gas could easily be dense enough to confine radio sources with $P \sim 10^{21}$–10^{22} W Hz^{-1}, and suggested that the absence of extended radio lobes in 'normal' elliptical galaxies was due to thermal confinement by this gas.

If the interstellar medium is important to the propagation of jets and the consequent formation of a radio source, this may also explain why the bulge luminosity of S0 galaxies, rather than their total luminosity, appears to be the important parameter influencing their radio emission. Any gas in the disc is cold and supported by rotation, while the density of hot nuclear gas is fixed by the mass of the bulge component. The major complication introduced by a disc is that some beams might plough into the cool disc gas, which could be dense enough to stop even the most powerful ones. Whether a radio source would form under these circumstances is an open question.

In strong radio galaxies, the inferred beam power correlates well with nuclear emission-line luminosity (Rawlings & Saunders 1987). Accepting our null hypothesis, and the notion that beams may escape from small galaxies without significant radio emission resulting, there should be a population of elliptical galaxies with strong emission lines but little radio emission. The optical activity might be violent, depending on orientation. Clearly, however, beams as powerful as those found in 3CR galaxies are rare.

All the galaxies in our sample have weak emission lines by these standards, and the lack of any dependence on radio power suggests that other sources of ionization are effective. However, the sample does contain objects like NGC 7213, a weak radio source which has broad permitted lines (Filippenko & Halpern 1984) and might be an example of an escaped beam.

Thus some qualitative understanding can be gained by focusing on the interaction between the radio beam and the interstellar medium. Such as approach does not require any detailed understanding of how beams are generated. It also poses some reasonably precise questions. For instance, we need to know whether the frequency of optical activity in early-type galaxies is consistent with the idea that all these galaxies have the same distribution of beam power. We also need to distinguish small, intrinsically weak sources from traces of the escape of powerful beams. This requires an estimate of the distribution of source power resulting from a given beam interacting with a given surrounding medium. This in turn would make detailed interpretation of the luminosity functions possible. One would also like to know whether Seyfert galaxies fit into such a scheme. Are they cases where a powerful beam has broken up in the

disc? Are other types of radio-quiet objects examples of an escaped beam? Systematic radio surveys at high resolution, searches for strong optical activity and detailed calculations are necessary to answer such questions.

References

Auriemma, C., Perola, G. C., Ekers, R., Fanti, R., Lari, C., Jaffe, W. J. & Ulrich, M. H., 1977. *Astr. Astrophys.*, **57,** 41.

Avni, Y. & Bahcall, J. N., 1980. *Astrophys. J.*, **235,** 694.

Avni, Y., Soltan, A., Tananbaum, H. & Zamorani, G., 1980. *Astrophys. J.*, **238,** 800.

Baum, S. A., 1987. *PhD thesis,* University of Maryland.

Bender, R., Döbereiner, S. & Möllenhof, C., 1987. *Astr. Astrophys.*, **177,** L53.

Bergvall, N. A. S., Ekman, A. B. G., Lauberts, A., Westerlund, B. E., Borchkhadze, T. M., Breysacher, J., Laustsen, S., Muller, A. B., Schuster, H.-E., Surdej, J. & West, R. M., 1978. *Astr. Astrophys. Suppl.*, **33,** 243.

Biermann, P. & Kronberg, P. P., 1983. *Astrophys. J.*, **268,** L69.

Binney, J., 1985. *Mon. Not. R. astr. Soc.*, **212,** 767.

Birkinshaw, M. & Davies, R. L., 1985. *Astrophys. J.*, **291,** 32.

Blandford, R. D. & Rees, M. J., 1978. *Phys. Scripta,* **17,** 265.

Brown, B. W. M., Hollander, M. & Korwar, R. M., 1974. In: *Reliability and Biometry,* p. 327, eds Proschan, F. & Serfling, R. J., Society of Industrial Applied Mathematics, Philadelphia.

Burns, J. O., Feigelson, E. D. & Schreier, E. J., 1983. *Astrophys. J.*, **273,** 128.

Caganoff, S., Ekers, R. D., Bicknell, G. V. & Carter, D., 1988. In: *Active Galactic Nuclei,* p. 137, eds Miller, H. R. & Witta, P. J., Springer-Verlag, Berlin.

Caldwell, N., 1984. *Publs astr. Soc. Pacif.*, **96,** 287.

Condon, J. J., Condon, M. A., Gisler, G. & Puschell, J. J., 1982. *Astrophys. J.*, **252,** 102.

Danziger, I. J. & Goss, W. M., 1983. *Mon. Not. R. astr. Soc.*, **202,** 703.

Davies, R. L., Efstathiou, G., Fall, S. M., Illingworth, G. & Schechter, P. L., 1983. *Astrophys. J.*, **266,** 41.

Diaconis, P. & Efron, B., 1983. *Sci. Am.*, **284**(5), 96.

Disney, M. J. & Cromwell, R. H., 1971. *Astrophys. J.*, **164,** L35.

Disney, M. J. & Wall, J. V., 1977. *Mon. Not. R. astr. Soc.*, **179,** 235.

Disney, M. J., Sparks, W. B. & Wall, J. V., 1984. *Mon. Not. R. astr. Soc.*, **206,** 899.

Dressel, L. L., 1981. *Astrophys. J.*, **245,** 25.

Dressel, L. L. & Condon, J. J., 1978. *Astrophys. J. Suppl.*, **36,** 53.

Dressler, A. & Sandage, A., 1983. *Astrophys. J.*, **265,** 664.

Ekers, R. D. & Ekers, J. A., 1973. *Astr. Astrophys.*, **24,** 247.

Ekers, R. D., Wall, J. V., Shaver, P. A., Goss, W. M., Fosbury, R. A. E., Danziger, I. J., Moorwood, A. F., Malin, D. F., Monk, A. S. & Ekers, J. A., 1989. *Mon. Not. R. astr. Soc.*, **236,** 737.

Fabbiano, G., Klein, U., Trinchieri, G. & Wielebinski, R., 1987. *Astrophys. J.*, **312,** 111.

Feigelson, E. D. & Nelson, P. I., 1985. *Astrophys. J.*, **293,** 192.

Filippenko, A. V. & Halpern, J. P., 1984. *Astrophys. J.*, **285,** 458.

Fomalont, E. B., Kellermann, K. I., Wall, J. V. & Weistrop, D., 1984. *Science,* **225,** 23.

Forman, W., Jones, C. & Tucker, W., 1985. *Astrophys. J.*, **293,** 102.

Franceschini, A., Danese, L., De Zotti, G. & Toffolatti, L., 1988. *Mon. Not. R. astr. Soc.*, **233,** 157.

Gunn, J. E., 1979. In: *Active Galactic Nuclei,* p. 213, eds Hazard, C. & Mitton, S., Cambridge University Press.

Habe, A. & Ikeuchi, S., 1985. *Astrophys. J.*, **289,** 540.

Halley, E., 1693. *Phil. Trans. R. Soc. Lond.*, **17,** 596.

Haynes, R. F., Cannon, R. D. & Ekers, R. D., 1983. *Proc. astr. Soc. Aust.*, **5,** 241.

Heeschen, D. S., 1970. *Astr. J.*, **75,** 523.

Humason, M. L., Mayall, N. U. & Sandage, A. R., 1956. *Astr. J.*, **61,** 97.

Hummel, E., 1981. *Astr. Astrophys.*, **93,** 93.

Hummel, E. & Kotanyi, C. G., 1982. *Astr. Astrophys.*, **106,** 183.

Hummel, E., Kotanyi, C. G. & Ekers, R. D., 1983. *Astr. Astrophys.*, **127,** 205.

Impey, C. D., Wynn-Williams, C. G. & Becklin, E. E., 1986. *Astrophys. J.*, **309,** 572.

Isobe, T., Feigelson, E. D. & Nelson, P. I., 1986. *Astrophys. J.*, **306,** 490.

Jenkins, C. R., 1983. *Mon. Not. R. astr. Soc.*, **205,** 1321.

Jenkins, C. R., 1984. *Astrophys. J.*, **277,** 501.

Jura, M., 1986. *Astrophys. J.*, **306,** 483.
Killeen, N. E. B., Bicknell, G. V. & Ekers, R. D., 1986. *Astrophys. J.*, **302,** 306.
Killeen, N. E. B., Bicknell, G. V. & Ekers, R. D., 1988. *Astrophys. J.*, **325,** 180.
Knapp, G. R., 1987. *Structure and Dynamics of Elliptical Galaxies, IAU Symp. No. 127,* p. 145, ed. de Zeeuw, T., Reidel, Dordrecht.
Kotanyi, C. G. & Ekers, R. D., 1979. *Astr. Astrophys.*, **73,** L1.
Lauberts, A., 1982. *The ESO/Uppsala Survey of the ESO(B) Atlas,* European Southern Observatory.
Leir, A. A. & van den Bergh, S., 1977. *Astrophys. J. Suppl.*, **34,** 381.
Lynden-Bell, D., 1987. *Q. J. R. astr. Soc.*, **28,** 187.
Meurs, E. J. A. & Wilson, A. S., 1984. *Astr. Astrophys.*, **136,** 206.
Mills, B. Y., 1981. *Proc. Astr. Soc. Aust.*, **4,** 156.
Mood, A. M., Graybill, F. A. & Boes, D. C., 1974. *Introduction to the Theory of Statistics,* p. 440, McGraw-Hill, New York.
Nulsen, P. E. J., Stewart, G. C. & Fabian, A. C., 1984. *Mon. Not. R. astr. Soc.*, **208,** 185.
O'Connell, R. W. & Dressel, L. L., 1978. *Nature,* **276,** 374.
Phillips, M. M., Jenkins, C. R., Dopita, M. A., Sadler, E. M. & Binette, L., 1986. *Astr. J.*, **91,** 1062.
Press, W. H., Flannery, B. P., Teukolsky, S. A. & Vetterling, W. T., 1986. *Numerical Recipes,* Cambridge University Press.
Rawlings, S. & Saunders, R., 1987. In: *Emission Lines in Active Galactic Nuclei,* p. 160, ed. Gondhalekar, P. M., Rutherford-Appleton Laboratory.
Rees, M. J., 1978. *Phys. Scripta,* **17,** 193.
Rieke, G. H., Lebofsky, M. J., Thompson, R. I., Low, F. J. & Tokunaga, A. T., 1980. *Astrophys. J.*, **238,** 24.
Rose, J. A., 1985. *Astr. J.*, **90,** 1927.
Sadler, E. M., 1982. *PhD thesis,* Australian National University.
Sadler, E. M., 1984a. *Astr. J.*, **89,** 23.
Sadler, E. M., 1984b. *Astr. J.*, **89,** 34.
Sadler, E. M., 1984c. *Astr. J.*, **89,** 53.
Sadler, E. M. & Gerhard, O. E., 1985. *Mon. Not. R. astr. Soc.*, **214,** 177.
Sandage, A. & Tammann, G. A., 1981. *A Revised Shapley–Ames Catalog of Bright Galaxies,* Carnegie Institution of Washington.
Sansom, A. E., Danziger, I. J., Ekers, R. D., Fosbury, R. A. E., Goss, W. M., Monk, A. S., Shaver, P. A., Sparks, W. B. & Wall, J. V., 1987. *Mon. Not. R. astr. Soc.*, **229,** 15.
Schmidt, M., 1968.*Astrophys. J.*, **151,** 393.
Schmidt, M. & Green, R. F., 1986. *Astrophys. J.*, **305,** 68.
Schmitt, J. H. M. M., 1985. *Astrophys. J.*, **293,** 178.
Siegel, S., 1956. *Non-Parametric Statistics,* McGraw-Hill, New York.
Smith, R. M. & Bicknell, G. V., 1986. *Astrophys. J.*, **308,** 36.
Tammann, G. A., 1977. In: *Supernovae: A Survey of Current Research,* p. 371, eds Rees, M. J. & Stoneham, R. J., Reidel, Dordrecht.
Terzian, Y., 1968. *Planetary Nebulae, IAU Symp. No. 34,* p. 87, eds Osterbrock, D. E. & O'Dell, C. R., Reidel, Dordrecht.
Thompson, A. R., Clark, B. G., Wade, C. M. & Napier, P. J., 1980. *Astrophys. J. Suppl.*, **44,** 151.
van den Bergh, S., McClure, R. D. & Evans, R., 1987. *Astrophys. J.*, **323,** 44.
Wall, J. V. & Peacock, J. A., 1985. *Mon. Not. R. astr. Soc.*, **216,** 173.
Wall, J. V., Shimmins, A. J. & Merkelijn, J. K., 1971. *Aust. J. Phys., Astrophys. Suppl.*, **19,** 1.
White, G. L., McAdam, W. B. & Jones, I. G., 1984. *Proc. astr. Soc. Aust.*, **5,** 507.
Wilkinson, A., Browne, I. W. A., Kotanyi, C., Christiansen, W. A., Williams, R. & Sparks, W. B., 1987. *Mon. Not. R. astr. Soc.*, **224,** 895.
Windhorst, R., 1984. *PhD thesis,* University of Leiden.

Appendix A: Luminosity functions and univariate survival analysis

Feigelson & Nelson (1985) and Schmitt (1985) recently introduced survival analysis to astronomers, although a notable early practitioner was Halley (1693). Here we concentrate on the application of survival analysis techniques to luminosity functions.

Suppose we have observed a representative sample of astronomical objects, each with true luminosity X_i, distance R_i, and apparent brightness $x_i\,(=X_i/f(R_i))$. When no detection is made

(i.e. x_i is below the sensitivity s_i of the survey for object i), the observation is said to be censored.

Evidently there is some information in the upper limits, and survival analysis techniques allow us to extract this information and recover the probability distribution function $\rho(X)$. The most commonly used estimator of ρ is the Kaplan–Meier estimator (Feigelson & Nelson 1985), which recovers the cumulative distribution function. A variant is the Fanti estimator described by Hummel (1981), which differs from the Kaplan–Meier only in its algebraic form. The Avni estimator (Avni *et al.* 1980) gives the differential distribution (and hence ρ) directly, binned into convenient ranges of X. Both the Kaplan–Meier and Avni estimators are maximum-likelihood estimators and hence are equivalent.

Since ρ estimates the distribution function, it is directly proportional to the luminosity function of X – the scaling factor will have the dimensions of objects per unit volume. In the absence of this scaling factor, ρ is often called the fractional luminosity function.

Under what conditions will the maximum likelihood estimators converge to the true function ρ? The basic condition for validity of the likelihood equations is that the true values X_i are statistically independent of the limits $s_i f(R_i)$. This is true if X is independent of the distance to an object; in other words, the luminosity function must be independent of distance. This is not too restrictive a condition for extragalactic objects at low redshifts where evolutionary effects are unimportant, but might cause problems in stellar work, for instance in studies of galactic structure.

Another precondition worth exploring is the requirement that the initial sample be representative. In astronomy this is often impossible. For example, a magnitude-limited sample of objects grossly misrepresents the true distribution of optical luminosities L. If the quantity of interest X is statistically dependent on L, the ρ estimated by survival analysis (or any other technique) will reflect the initial biased distribution of L. The maximum-likelihood estimators have a further problem: in a magnitude-limited sample, L correlates with distance R. If L also correlates with X, the upper limits and true values are no longer independent, violating the condition for the use of these estimators.

For this reason, it is necessary to use a 'semi-bivariate' estimator $\rho(X, L)$ in many cases. The data are binned into small ranges of L to weaken the X–L dependence. This gives a useful estimate of the distribution of X at various L, but ρ cannot be used to estimate the distribution of L. The exact size of the L bins must be decided empirically, using Monte Carlo simulations.

It is vital to know the size of the statistical errors on the estimators. Asymptotic formulae have been derived, but in practice one does not know whether the asymptotic limit has been reached. Effects like the finite size of the L bins must also be accounted for. An obvious way of evaluating the errors is by a direct Monte Carlo simulation. Another method, often less laborious, uses a bootstrap (Diaconis & Efron 1983) on the original list of x_i, s_i, X_i, R_i and L_i. Our experiments, using the luminosity functions derived in this paper, show that Monte Carlo estimates of variances agree well with results from bootstrapping.

Error estimates on distributions are most easily portrayed and understood using a binning method like that of Avni *et al.* (1980). In this case, our simulations show that adjacent bins have largely independent errors. A cumulative distribution like the Kaplan–Meier has strongly correlated errors which can be very misleading.

Finally, the use of upper limits can often improve the signal-to-noise ratios on estimates of luminosity functions. In some Monte Carlo experiments, we found that the size of the random errors did not rise as quickly as one would expect purely on the basis of a declining detection rate; that is, the upper limits were doing useful work in keeping up the signal-to-noise ratio. Greenwood's formula (Feigelson & Nelson 1985) for the error on the Kaplan–Meier estimator is consistent with this observation.

Appendix B. Estimation of a bivariate luminosity function by survival analysis

Schmitt (1985) derived a two-dimensional analogue of the one-dimensional maximum-likelihood Avni estimator. The data are binned into cells in the two variables of interest: call these X and Y and index the cells by the pair of integers i, j where $i=1,2,\ldots N$ and $j=1,2,\ldots M$. The probability in each cell is then $f_{i,j}$, and the maximum likelihood condition results in a set of $M\times N$ equations of the form

$$\mathscr{F}_{i,j}(\ldots f_{k,l}\ldots)=0, \qquad \text{where } i=1,2,\ldots N, j=1,2,\ldots M, \tag{B1}$$

where the constraint

$$\sum_{i=1}^{N}\sum_{j=1}^{M} f_{i,j}=1 \tag{B2}$$

has been applied in the maximization. Each of the functions $\mathscr{F}$ is identical in form and depends on four quantities: $N_{i,j}$, the number of detections of X and Y in the cell (i,j); $U1_{i,j}$, the number of upper limits in X and detections of Y; $U2_{i,j}$, the number of upper limits in Y and detections of X; and $U3_{i,j}$, the number of upper limits in both X and Y. The total number of observations is $N_{\rm tot}$. In two dimensions, each of the $\mathscr{F}_{i,j}$ take the form

$$N_{i,j}+f_{i,j}\times\left\{\sum_{k=1}^{i}\frac{U1_{k,j}}{\Sigma_{l=k}^{M}f_{l,j}}+\sum_{k=1}^{j}\frac{U2_{i,k}}{\Sigma_{l=k}^{N}f_{i,l}}+\sum_{k=1}^{i}\sum_{k'=1}^{j}\frac{U3_{k,k'}}{\Sigma_{l=k}^{M}\Sigma_{l'=k'}^{N}f_{l,l'}}-N_{\rm tot}\right\}=0, \tag{B3}$$

which, in one dimension, simplifies to

$$N_i+g_i\left\{\sum_{k=1}^{i}\frac{U1_k}{\Sigma_{l=k}^{M}g_l}-N_{\rm tot}\right\}=0 \tag{B4}$$

if X, for example, is the variable of interest. Associated with a solution $f_{i,j}$ is an entropy

$$S_2=-2\log\mathscr{L}(\ldots f_{k,l}\ldots), \tag{B5}$$

where $\mathscr{L}$ is the likelihood function.

Schmitt's discussion of these equations (in appendices to the paper) is rather brief, and some typographical errors and elisions make the argument difficult to follow. However, the important points are simple and elegant. If the estimate of the bivariate function $f_{i,j}$ can be factorized into separate dependences on X and Y,

$$f_{i,j}=g_ih_j, \tag{B6}$$

then the maximum-likelihood estimate of the g_i and h_j is given by the appropriate one-dimensional Avni equations (Schmitt does not show this explicitly). It follows that one can calculate a

one-dimensional entropy for the problem to hand from the product of the one-dimensional likelihoods

$$S_1 = -2\log[\mathscr{L}(\ldots g_k \ldots)\times\mathscr{L}(\ldots h_l \ldots)], \tag{B7}$$

and the likelihood ratio

$$\Delta = S_1 - S_2 \tag{B8}$$

is asymptotically χ^2 with $MN - M - N$ degrees of freedom (e.g. Mood, Graybill & Boes 1974). The statistic Δ is an excellent candidate for use in a general test of statistical association between the variables X and Y.

The generality of the method encourages one to proceed with the rather complex business of obtaining a solution to equation (B3), calculating the entropies and eventually using the test of equation (B8). However, unlike the one-dimensional analogue, equation (B3) is not known to have a solution in a closed form. Schmitt proposed an iterative method of solution, but our empirical experience (in Monte Carlo experiments) is that iteration does not in general converge to the correct answer, though changes in the apparent solution can become very slow. We examined the one-dimensional case in some detail, since Schmitt's result on factorizability shows that any results for the one-dimensional case will apply to two-dimensional factorizable cases. In one dimension, an exact solution can be calculated for comparison. Even in this simple case, the empirical result is that iteration need not converge.

Some analytical progress in examining the problem is also possible. Consider iteration number n. The current solution equals the true solution, plus a (presumably) small error ε:

$$g_i^{(n)} = g_i^{(\mathrm{true})} + \varepsilon_i^{(n)}. \tag{B9}$$

Substituting this into the one-dimensional form given by equation (B4), and expanding to first order, we see that the prospects for convergence are poor. For example, if at step n a particular $\varepsilon_k^{(n)}$ is non-zero, at step $n+1$ *all* the error terms will be finite. The iterative method tends to converge to $g_i^{(\infty)} = 0$, at least for values of i where the presence of upper limits affects the solution. The values of $\varepsilon_k^{(n)}$ often become large and the iteration settles down at a bogus solution where the probabilities may even become negative.

Discouraged by these results, we resorted to direct numerical solution of equation (B3). Various methods of solving the $M \times N$ coupled non-linear equations are possible. We chose to write the single equation

$$\sum_{i=1}^{N}\sum_{j=1}^{M}\mathscr{F}_{i,j}^2(\ldots f_{k,l}\ldots) = 0 \tag{B10}$$

so that the solution can be found by minimizing this sum of squares with respect to the $M \times N$ variables $f_{k,l}$. Efficient numerical methods exist for such problems, though they have to be used cautiously (e.g. Press *et al.* 1986, p. 272), with the obvious check that each of the equations (B3) is satisfied at the minimum. We used the routine E04GBF from the library of the Numerical Algorithms Group, and found it satisfactory for M and N less than about 10.

Calculating the one-dimensional distributions g_i and h_j (equation B6) for use in (B7) is straightforward, as the equations can be solved recursively (Avni *et al.* 1980). There are, however, a number of rather intricate practical problems connected with a satisfactory solution of the two-dimensional problem. It is not appropriate to discuss them in detail here, but we give some indication of their nature.

The normalization condition (B2) is the main difficulty. If the arrays of data $N_{i,j}$, $U1_{i,j}\ldots$ are such that the arrays 'end' with limits rather than detections, then inspection of equation (B3), or

intuition, shows that normalization cannot hold. This is most obvious in the one-dimensional case. However, if (B2) is violated, the numerical solution fails and the entropy S_2 (equation B5) is infinite. To ensure a sensible result, it is necessary for the arrays to 'end' in detections.

This can be achieved by changing the one of the appropriate 'last' limits into a detection. It amounts to changing the 'last' cell size until it extends to values of X or Y which correspond to the actual, albeit unknown, values belonging to one of the objects in the sample. Since the cell sizes are correspondingly unknown, the probabilities in affected cells are of no use in estimating the bivariate function $f_{i,j}$. Nevertheless, a sensible value for the entropy can now be obtained. Although it may seem paradoxical to regard a change from an infinite to a finite value as meaningful, the point is that a problem which violates normalization is physically unrealistic (assuming the variables X and Y are necessarily finite) and badly posed. Small adjustments to the arrays produce a well-posed problem which is physically identical to the original and has the merit of possessing a solution, although not all of the solution (the probabilities in the 'last' cells) can be used.

In this discussion, 'end' and 'last' have been used in quotation marks because this usage is rather free for a two-dimensional array, although the meaning is obvious from the basic equations (B3). The novelty introduced in two dimensions is the array $U3_{i,j}$ of doubly censored data. It sometimes happens that an array 'ends' in doubly-censored observations. Changing these into detections can amount to a radical change in sizes of cells. In such cases one may choose to add in a fictitious detection, or leave out the offending censored point, in the interests of not disrupting the binning scheme too much. One then obtains a solution of a problem which is in some sense adjacent, but not identical, to the original one.

Rearrangement of 'last' detections and limits to give a well-posed problem has consequences for the factorization expressed by equation (B6). This factorization may be destroyed by some changes in cell size, and for this reason in particular the doubly-censored data may give difficulty. On the other hand, factorizability of the *estimate* $f_{i,j}$ of the true bivariate function $f_{i,j}^{(\mathrm{true})}$ only indicates in a statistical sense whether the true function will factorize. For instance, $f_{i,j}=0$ if there happens to be no detection in cell (i,j), and for a sparsely populated array of detections it can easily happen that $g_i \neq 0$ and $h_j \neq 0$ when $f_{i,j}=0$, even if $f_{i,j}^{(\mathrm{true})}$ is factorizable.

The size of the cells used can also affect the result, as Schmitt discusses. Coarse binning may mean that a biased estimate of $f_{i,j}^{(\mathrm{true})}$ is recovered. In principle, the bins can be made arbitrarily small to avoid this problem, but numerical solution becomes difficult for large values of M and N.

As a final complication, the distribution of the statistic Δ (equation B8) is only known to be χ^2 asymptotically. Also, the number of degrees of freedom $MN-M-N$ is often a random variable, since one might fix the size of the array *a posteriori* to include all the detections that happened to have been made.

The correct approach is to realize that Schmitt's test using Δ gives a useful statistic for discovering whether the underlying bivariate distribution is factorizable, which in turn is the most general test of statistical association between X and Y. However, the test is not non-parametric in real situations. The distribution of Δ, on the null hypothesis that the underlying distribution factorizes, must be found by Monte Carlo simulations. These simulations should use the same set of rules for determining the size of cells, M and N, and ensuring normalization, as used in examination of the actual data. The whole set of problems discussed above can be absorbed into the distribution of Δ, regarded as a statistic whose probable usefulness is indicated by likelihood theory. Such simulations will also produce useful estimates of how reliable the estimate of the bivariate function might be, and many other statistics of interest.

One may also use a bootstrap simulation to achieve some of the same results, for example, variances on the estimates of the bivariate function. This is easier than a Monte Carlo simulation, since one can use the actual data rather than setting up an elaborate model, but the distribution of Δ under the null hypothesis cannot be obtained by a bootstrap. The results from both methods usually agree well, but with a bootstrap there is some risk of an absurd result for a particular estimate (see, for instance, Diaconis & Efron 1983). The bootstrap may also fail to give a sensible answer for variances on the estimates of quantiles, particularly if the detection rate is low.